Progress in Oceanography 154 (2017) 1–24

Contents lists available at ScienceDirect

Progress in Oceanography

journal homepage: www.elsevier.com/locate/pocean

Can neap-spring tidal cycles modulate biogeochemical fluxes in the abyssal near-seafloor water column?

Robert Turnewitsch [a,*], Andrew Dale [a], Niko Lahajnar [b], Richard S. Lampitt [c], Kei Sakamoto [d]

[a] Scottish Association for Marine Science (SAMS), Oban PA37 1QA, United Kingdom
[b] University of Hamburg, Institute for Geology, Bundesstraße 55, D-20146 Hamburg, Germany
[c] National Oceanography Centre Southampton (NOCS), Southampton SO14 3ZH, United Kingdom
[d] Meteorological Research Institute, Oceanography and Geochemistry Research Department, 1-1 Nagamine, Tsukuba, Ibaraki 305-0052, Japan

ARTICLE INFO

Article history:
Received 11 September 2016
Received in revised form 9 March 2017
Accepted 5 April 2017
Available online 21 April 2017

Keywords:
Neap-spring tide
Sediment trap
Biogeochemical flux
Boundary layer
Abyssal ocean

ABSTRACT

Before particulate matter that settles as 'primary flux' from the interior ocean is deposited into deep-sea sediments it has to traverse the benthic boundary layer (BBL) that is likely to cover almost all parts of the seafloor in the deep seas. Fluid dynamics in the BBL differ vastly from fluid dynamics in the overlying water column and, consequently, have the potential to lead to quantitative and compositional changes between primary and depositional fluxes. Despite this potential and the likely global relevance very little is known about mechanistic and quantitative aspects of the controlling processes. Here, results are presented for a sediment-trap time-series study that was conducted on the Porcupine Abyssal Plain in the abyssal Northeast Atlantic, with traps deployed at 2, 40 and 569 m above bottom (mab). The two bottommost traps were situated within the BBL-affected part of the water column. The time series captured 3 neap and 4 spring tides and the arrival of fresh settling material originating from a surface-ocean bloom. In the trap-collected material, total particulate matter (TPM), particulate inorganic carbon (PIC), biogenic silica (BSi), particulate organic carbon (POC), particulate nitrogen (PN), total hydrolysable amino acids (AA), hexosamines (HA) and lithogenic material (LM) were determined. The biogeochemical results are presented within the context of time series of measured currents (at 15 mab) and turbidity (at 1 mab). The main outcome is evidence for an effect of neap/spring tidal oscillations on particulate-matter dynamics in BBL-affected waters in the deep sea. Based on the frequency-decomposed current measurements and numerical modelling of BBL fluid dynamics, it is concluded that the neap/spring tidal oscillations of particulate-matter dynamics are less likely due to temporally varying total free-stream current speeds and more likely due to temporally and vertically varying turbulence intensities that result from the temporally varying interplay of different rotational flow components (residual, tidal, near-inertial) within the BBL. Using information from previously published empirical and theoretical relations between fluid and biogeochemical dynamics at the scale of individual particle aggregates, a conceptual and semi-quantitative picture of a mechanism was derived that explains how the neap/spring fluid-dynamic oscillations may translate through particle dynamics into neap/spring oscillations of biogeochemical aggregate decomposition (microbially driven organic-matter breakdown, biomineral dissolution). It is predicted that, during transitions from neap into spring tides, increased aggregation in near-seafloor waters and/or reduced deposition of aggregates at the seafloor coincides with reduced biogeochemical particulate-matter decomposition in near-seafloor waters. By contrast, during transitions from spring into neap tides, enhanced biogeochemical particulate-matter decomposition in near-seafloor waters is predicted to coincide with increased deposition of particulate matter at the seafloor. This study suggests that, in addition to current speed, the specifics and subtleties of the interplay of different rotational flow components can be an important control on how the primary flux from the interior ocean is translated into the depositional flux, with potential implications for sedimentary carbon deposition, benthic food supply and possibly even the sedimentary records of environmental change.
© 2017 The Authors. Published by Elsevier Ltd. This is an open access article under the CC BY license (http://creativecommons.org/licenses/by/4.0/).

* Corresponding author.
E-mail addresses: robert.turnewitsch@sams.ac.uk (R. Turnewitsch), niko.lahajnar@zmaw.de (N. Lahajnar), r.lampitt@noc.ac.uk (R.S. Lampitt), ksakamot@mri-jma.go.jp (K. Sakamoto).

http://dx.doi.org/10.1016/j.pocean.2017.04.006
0079-6611/© 2017 The Authors. Published by Elsevier Ltd.
This is an open access article under the CC BY license (http://creativecommons.org/licenses/by/4.0/).

1. Introduction

Deep-sea sediments constitute one of the main biogeochemical compartments of the Earth system and are a net carbon sink for ocean and atmosphere (Berner, 2004; Kump et al., 2004). Moreover, they provide food supply to almost all organisms living in the seafloor (Gage and Tyler, 1991) and are a crucial recorder of environmental change. Consequently, an in-depth understanding of the processes involved in the formation of deep-sea sediments is essential.

Quantitatively important vehicles for the transport of particulate material from the surface into the deep interior ocean, and from the interior ocean into the near-seafloor waters (the 'primary flux'), are phytodetrital particle aggregates and zooplankton faecal pellets (e.g., Rowe and Staresinic, 1979; Turner, 2002, 2015). Before settling particulate material from the surface and interior ocean is finally deposited in sediments, it has to traverse the "benthic transition zone" (Honjo et al., 1982), i.e., the lower part of the oceanic water column in which the presence of the seafloor has a detectable direct or indirect influence on physical, chemical, biological and/or sedimentological aspects (Fig. 1) (Boudreau and Jørgensen, 2001). Lampitt et al. (2000) pointed out that the "role of the benthopelagic layer [which can be viewed as another term for the 'benthic transition zone'] relative to that of the sediment/water interface (SWI) and sediment mixed layer has been largely neglected". This is despite the fact that there is "no a priori reason why this layer might not be a region of high biogeochemical activity" (Rutgers van der Loeff and Boudreau, 1997). Moreover, the specifics and subtleties of boundary-layer fluid dynamics can control aspects of early diagenesis of organic matter in surface sediments ("breathing sediments": Lorke et al., 2003).

It has been argued that the potential biogeochemical importance of boundary-layer processes results from an increase of the residence time of particulate matter in the near-seafloor waters as compared to the residence time in a corresponding layer of water of the same thickness in the interior ocean. This increase leaves more time for microbially driven breakdown of organic matter and dissolution of biogenic minerals such as calcite and biogenic silica to act upon the particles before final deposition in the underlying sediments. [In this paper, the term 'biogeochemical decomposition' is used to describe microbially driven decay of organic matter, leaching and dissolution of biogenic minerals, but not physical disaggregation.] The increased residence times of the particulate matter are thought to be due to increased turbulence intensities near the seafloor (Fig. 1a) (e.g., Wimbush and Munk, 1970; Gust and Weatherly, 1985; Gross et al., 1986; Taylor and Sarkar, 2007; Sakamoto and Akitomo, 2009). This is because turbulent overturns might have a direct 'suspending' effect on the particle aggregates and/or an indirect effect through gradual breakdown of larger faster settling aggregates into smaller more slowly settling aggregates or even primary particles, thereby reducing net settling speeds. In addition, it has been argued that increased turbulence intensities might also directly affect rates of biogeochemical reactions in near-seafloor waters (Karp-Boss et al., 1996; Rutgers van der Loeff and Boudreau, 1997).

Main parts of the benthic transition zone or benthopelagic layer are illustrated in Fig. 1. The part of the near-seafloor water column where the presence of the seafloor has a detectable influence on fluid dynamics is the benthic or bottom boundary layer (BBL). The BBL typically overlaps with a near-seafloor layer in which seawater turbidity is increased; this latter layer is called benthic or bottom nepheloid layer (BNL). Maintenance of the BNL is thought to require repeated "recirculation" of particulate matter in near-seafloor waters. Some of this recirculating material will have been in transient contact with the seafloor. In this context, the term 'resuspension' is used for particles that were already deposited at the seafloor for some time and may have become part of the more consolidated surface sediment, whereas the term 'rebounding' is used for particles that were recently and transiently in contact with the seafloor but had not yet become part of the more consolidated sur-

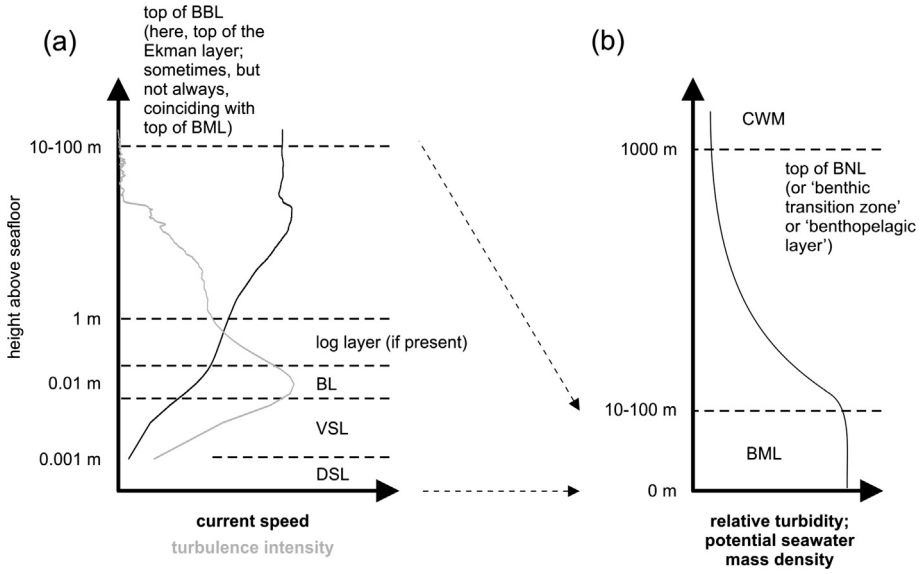

Fig. 1. Different ways of describing the vertical structure of the near-seafloor water column above a flat seafloor in the deep sea. (a) Structure of the near-seafloor water column according to the shapes of the profiles of current speed and turbulence intensity. BBL: bottom or benthic boundary layer (the part of the water column whose fluid dynamics are influenced by the ocean currents interacting with the seafloor). VSL: viscous sublayer (VSL). BL: buffer layer (transition between the log layer and the VSL). DSL: diffusive sublayer. All heights above the seafloor are only given as order-of-magnitude values. (b) Structure of the near-seafloor water column according to the vertical distribution of turbidity and/or potential mass density of seawater. CWM: clear water minimum (region within the interior ocean where turbidity reaches minimum values). BNL: bottom or benthic nepheloid layer (region above the seafloor where turbidity values are in excess of the CWM value). BML: bottom or benthic mixed layer (region above the seafloor where turbidity and mass-density values reach their maxima and where the values of these parameters are vertically largely invariable). The BNL is probably mechanistically and conceptually identical with what some researchers call the 'benthic transition zone' or 'benthopelagic layer' (mainly from a biological and/or biogeochemical perspective).

face sediment (Walsh et al., 1988; Gardner and Walsh, 1990; Walsh, 1992). It would seem likely that there is also a mixed form of resuspension (RS) *and* rebounding (RB): when rebound aggregates touch the SWI, particles that were already deposited may stick to the surfaces of the rebound aggregates and be carried into the near-seafloor waters together with the rebounding aggregates. Henceforth, this mixed process will be abbreviated as RS&RB.

The processes that maintain BNLs are not always clear. There are, however, four lines of independent evidence that suggest higher-frequency fluid dynamics due to tides (and possibly near-inertial oscillations) are required to sustain BNLs. (1) Rapidly settling particle aggregates co-exist with suspended (non-settling or very slowly settling) particles (McCave, 1986; Gardner et al., 1985; Walsh et al., 1988; Walsh and Gardner, 1992; Lampitt et al., 2000). As settling aggregates seem to be a quasi-continuous feature of near-seafloor waters and given their settling speeds, there must also be quasi-continuous or higher-frequency processes that operate on time scales of hours and/or shorter to act upon the particulate matter in ways that help retain and/or replenish a significant fraction of this material within the near-seafloor waters. (2) Given observed current speeds in the deep oceans (e.g., Fig. 1 of Turnewitsch et al., 2013; and Fig. 2a), critical current speeds for rebound (approximately $\geq$7 cm s^{-1} at 1 mab; Lampitt, 1985; Beaulieu, 2002) are not unusual in many regions of the deep sea. In this context, it is important to note that, in many deep-sea settings, tidal current-velocity oscillations push the total current speeds above the critical speed threshold for rebound (Turnewitsch et al., 2013). (3) Further evidence for the modulating influence of tides on particle dynamics in near-seafloor waters of the deep sea comes from turbidity time series that showed that there are times and/or environmental settings where turbidity at O(0.1–1 mab) varies at a tidal frequency. This was observed in fluid-dynamically more vigorous Deep Western Boundary Currents (e.g., Pak, 1983; Gross et al., 1986) as well as on the fluid-dynamically more quiescent eastern sides of ocean basins (Lampitt, 1985; Vangriesheim and Khripounoff, 1990; Auffret et al., 1994; Vangriesheim et al., 2001; Turnewitsch et al.: unpublished data from the Cape Verde Rise). (4) Finally, the deduced range of time scales that are critical for the maintenance of BNLs has also been indirectly confirmed by the presence of radioactive disequilibria (radioactivity ratios <1) between the highly particle-reactive and short-lived radioactive thorium-234 (^{234}Th) daughter nuclide (half life: 24.1 d) and the non-particle-reactive (chemically conservative) and extremely long-lived radioactive uranium-238 (^{238}U) parent nuclide (half life: 4.468×10^9 yr) in near-seafloor waters in a number of locations in the deep sea (Bacon and Rutgers van der Loeff, 1989; DeMaster et al., 1991; Turnewitsch and Springer, 2001; Turnewitsch et al., 2008; R. Turnewitsch: unpublished data from the abyssal Arabian Sea and Cape Verde Rise). Given the short half-life of ^{234}Th, the scavenging and settling processes that cause the radioactive disequilibria must occur on equally short or even shorter time scales.

The few studies that aimed to quantify biogeochemical BNL effects of increased residence times of particulate matter in the benthic transition zone concluded that up to several 10s of percent of the incoming primary flux might decompose in the near-seafloor waters that are controlled by BNLs and especially BBLs (Smith et al., 1986; Smith, 1992; Boetius et al., 2000; Walsh, 1992; Rutgers van der Loeff and Boudreau, 1997). This would be a significant fraction of the primary flux that is not depositing carbon and food into the sediments and that is not translated into the sedimentary record.

Overall, the existing evidence suggests that (1) higher-frequency (tidal, near-inertial) BBL fluid dynamics are an important driver for the maintenance of BNLs and the increase of residence times of particulate matter in near-seafloor waters; and (2) the increased residence times may result in up to several 10s of percent of the incoming primary particle flux to decompose before the remainder is deposited into the sediments.

In previous deep-sea boundary-layer studies, biogeochemical aspects and particle- and fluid-dynamic ones were treated largely separately. Here, we present a study that combines evidence from field studies of biogeochemical fluxes, currents and turbidity with numerical modelling of BBL fluid dynamics and previously published information on empirical or theoretical relations between fluid dynamics and biogeochemical fluxes at the scale of individual particle aggregates to search for a mechanistic link between biogeochemistry and fluid dynamics in an abyssal BBL, with the specific aim of shedding more light on the effect of higher-frequency fluid-dynamic oscillations on biogeochemical fluxes in near-seafloor waters of the deep sea. The study finds evidence for an imprint of the neap/spring tidal cycle on particulate-matter dynamics in a deep-sea BBL and develops the picture of a conceptual and semi-quantitative mechanism that translates these oscillations into neap/spring cycles of biogeochemical decomposition of particulate material in near-seafloor waters of the deep sea.

2. Material and methods

2.1. Sediment-trap time series: sampling and analyses

The samples for this study were collected as part of cruise 260 of RV Poseidon (26 April – 23 June 2000). The study area is located in the temperate Northeast Atlantic on a flat part of the Porcupine Abyssal Plain (PAP). Settling particulate material was collected by three sediment traps. One 'Kiel-type' trap was mounted on a benthic lander (BENGAL-lander FFB-01), with the opening of the trap at a nominal height above the seafloor of 2 m. The lander was deployed at 48°49.89′N, 16°31.80′W (48.832°N, 16.530°W) where the water depth at the seafloor is 4808 m. The other two traps of the Mark 7 type (McLane Research Laboratories, USA, MK7G-21 ITC Sediment Trap Operation Program V2.02) were deployed on a mooring at 48°49.59′N, 16°30.11′W (48.827°N, 16.502°W) where the water depth at the seafloor is 4802 m. The mooring traps were deployed at nominal heights above the seafloor of 40 mab (BENGAL-Deep) and 569 mab (BENGAL-Shallow). BENGAL-lander (2 mab) was collecting for 6×7 days from 08/05/2000 01:00 UTC until 19/06/2000 01:00 UTC, and BENGAL-Deep (40 mab) and BENGAL-Shallow (569 mab) were collecting for 7×7 days from 01/05/2000 01:00 UTC until 19/06/2000 01:00 UTC.

Recovered samples were stored at 4 °C until initial processing on board, which was carried out within 12 h after trap retrieval. Initial processing included macroscopic examination (Turnewitsch et al., 2015). The samples consisted almost completely of phytodetritus and did not contain any significant amounts of particles larger than ~1 mm; small faecal pellets only occurred in trace amounts (<10%).

After removal of the supernatant from the collection cups, particulate matter was split in a rotary sample splitter. Different splits were allocated to analyses of total settling particulate matter (TPM), particulate organic carbon (POC), particulate nitrogen (PN), total and individual hydrolysable amino acids (AA), the amino sugars or hexosamines (HA) glucosamine (Gluam) and galactosamine (Galam), stable-nitrogen-isotope composition of organic matter (δ^{15}N), particulate inorganic carbon (PIC: here, mainly calcite), biogenic silica (BSi, opal), and lithogenic material (LM).

Total carbon, POC and PN were analysed with a Carlo Erba NA-1500 Elemental Analyzer (Verardo et al., 1990; Nieuwenhuize et al., 1994). PIC was calculated by subtraction of POC from total carbon. BSi was measured according to Mortlock and Froelich

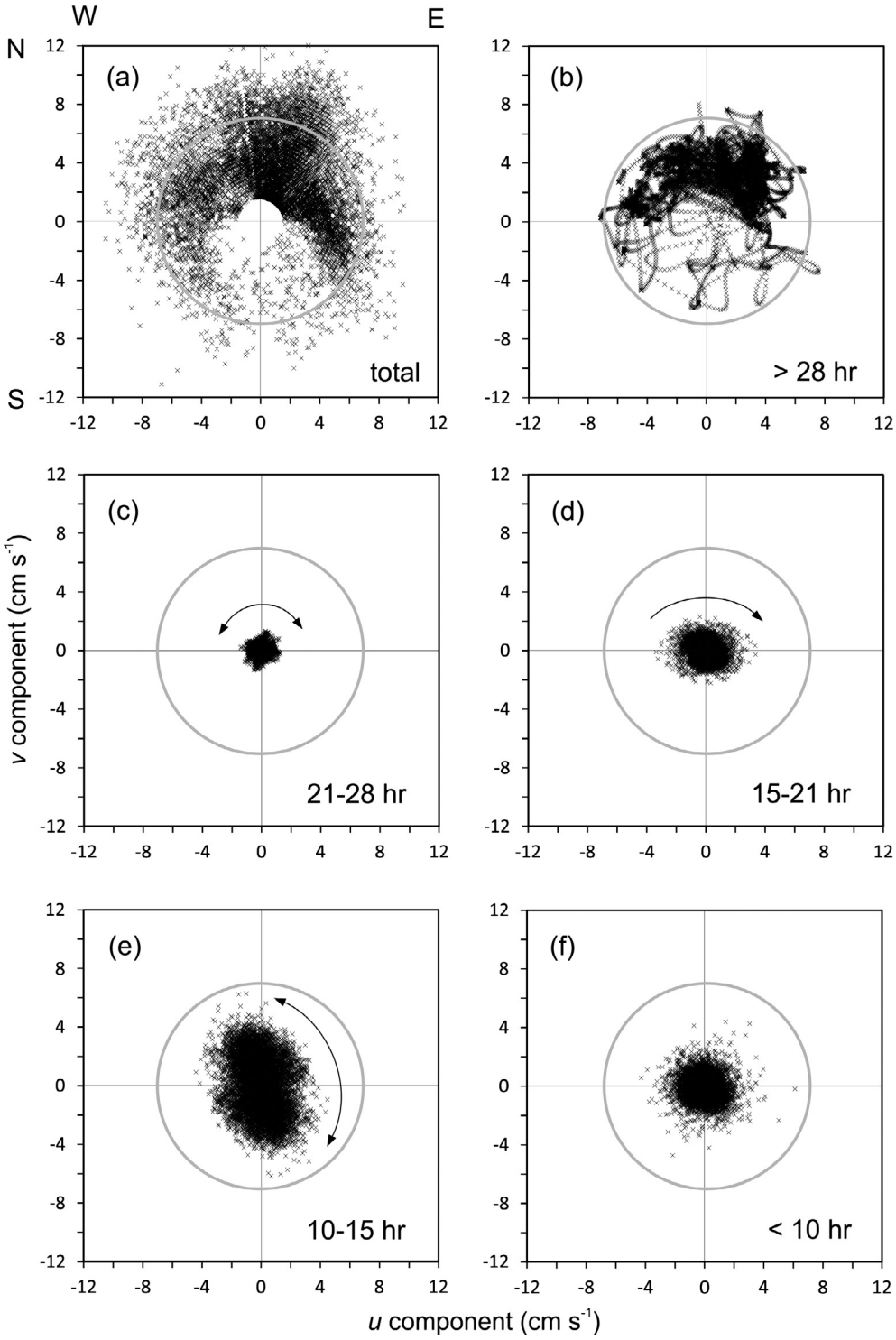

Fig. 2. (a) Total current velocity at 15 mab as measured by Vangriesheim et al. (2001) above the Porcupine Abyssal Plain (PAP) at 48.934°N, 16.532°W. Velocities are expressed in terms of their u (E-W) and v (N-S) components and were recorded hourly between 30 July 1996, 08:00 UTC, and 22 October 1997, 11:00 UTC. Grey circle: approximate critical near-seafloor current speed for rebounding phytodetritus (Lampitt, 1985; Beaulieu, 2002). (b)–(f) Current-velocity components resulting from a period-band analysis of the time series of total current velocity in (a). (b) Period of velocity oscillations >28 h ('lower-frequency'). (c) Period of velocity oscillations 21–28 h. This interval contains and is dominated by diurnal tidal oscillations. Sometimes the rotation of the measured current vector is counterclockwise (as expected from the TPXO model), sometimes it is clockwise. (d) Period of velocity oscillations 15–21 h. This interval contains and is dominated by near-inertial oscillations, with the measured current vector almost always rotating clockwise. (e) Period of velocity oscillations 10–15 h. This interval contains and is dominated by semidiurnal tidal oscillations. As with diurnal flow components, sometimes the rotation of the measured current vector is counterclockwise (as expected from the TPXO model) and sometimes it is clockwise. (f) Period of velocity oscillations <10 h. There is no rotational trend.

(1989), with slight modifications. LM was calculated as the remaining part of a sample after subtracting PIC, organic-matter (POC × 1.8) and BSi. AAs and HAs were analysed with a Pharmacia LKB Alpha Plus 4151 Amino Acid Analyser. Sediment samples were hydrolysed with 6 N HCl for 22 h at 110 °C. After hydrolysation samples were evaporated and taken up in acidic buffer (pH 2.2),

separated by cation exchange resin and detected fluorometrically after post-column derivatization (Lahajnar et al., 2007). Stable nitrogen isotopes were analysed on a Finnigan MAT 252 isotope ratio mass spectrometer after high-temperature flash combustion in the Carlo Erba NA-2500 elemental analyzer at 1100 °C (Gaye-Haake et al., 2005). Results are reported in the $\delta^{15}N$ notation (in ‰). Pure tank N_2 calibrated against the reference standards IAEA-N-1 and IAEA-N-2 of the International Atomic Energy Agency was used as a standard. Analytical precision was better than 0.1‰ for reference-standard material while duplicate measurements of samples typically yield a mean deviation of 0.2‰.

2.2. Physical-oceanographic, turbidity and fluid-dynamic information

Unfortunately, there is no current-meter time series available that corresponds to the sediment-trap time series. However, output from the TPXO barotropic tidal model of Egbert and Erofeeva (2002) gives sufficiently robust information on the timing of semidiurnal and neap/spring tidal oscillations during the sediment-trap time series. Moreover, there is a comprehensive time-series dataset of current velocities for the study area that was acquired in 1996/97 and discussed by Vangriesheim et al. (2001). The current meter (Aanderaa RCM8) was suspended above a benthic lander at a nominal height above the seafloor of 15 m at 48°56.06′N, 16°31.93′W (48.934°N, 16.532°W), recording vector-averaged hourly bins from 08:00 UTC on 30 July 1996 to 11:00 UTC on 22 October 1997. The resulting time series has been decomposed into five period bands, of less than 10, 10–15, 15–21, 21–28, and more than 28 h, by sequential application of a 6th order, low-pass Butterworth filter. The second of these bands is dominated by semidiurnal tides. The third band contains near-inertial variability, and the fourth contains the diurnal tidal signal. The measured current speeds and directions were compared with predictions of the TPXO model.

Vangriesheim et al. (2001) also measured turbidity levels with an IFREMER prototype nephelometer at a nominal height above the seafloor of 1 m. This nephelometer was operating during the aforementioned current-meter deployment in 1996/97. Furthermore, it was also operating from 4 March until 29 September 1998 at 48°56.52′N, 16°25.74′W (48.942°N, 16.429°W). However, there are no current-meter data for this second nephelometer deployment. But both nephelometer data sets can still be compared with corresponding output from the TPXO model. Furthermore, for an interval of ~ 18 days in mid July 1997, twelve repeat deployments of a CTD and transmissometer were carried out, allowing for identification of bottom mixed layers (BMLs) and their thicknesses (Turnewitsch and Springer, 2001).

To better understand the effects of an oscillating (tidal) flow component on aspects of BBL fluid dynamics, we revisited the data sets of Sakamoto and Akitomo (2009) who used a numerical model to investigate a tidally induced BBL in a rotating frame. The initial water column was weakly mass-density-stratified (the Richardson number $Ri = N_\infty^2/\omega^2$ was only 47.5, where N_∞ is the initial buoyancy frequency in the free-stream waters above the boundary layer and ω is the frequency of the tidal oscillations). Ten different scenarios were investigated. Seven of them (A-F, St) had the same tidal current-speed amplitude U_{tide}, but differed in terms of the temporal Rossby number $Ro_t = |\omega/f|$ and the thickness scale of the tidally induced BBL, $\delta = u_\tau/|f + \omega|$, where f is the latitudinally dependent Coriolis parameter, and $u_\tau = (\tau/\rho)^{0.5}$ is the shear velocity at the seafloor (where τ is the shear stress at the seafloor and ρ is the mass density of the water). For case A, B, C, D, E and F, Ro_t was 0.5, 0.8, 0.95, 1.05, 1.2 and 2.0, respectively. That is, for a given tidal frequency, these six scenarios revealed the influence of different rates of rotation (geographical latitude) on the geometry and dynamics of an oscillating BBL. For the St (Stokes) scenario, $Ro_t = \infty$ as $f = 0$ (equator scenario where the BBL oscillates but does not rotate). An additional eighth scenario was a pure Ekman boundary layer (Ek) in which the BBL rotates but does not oscillate ($\omega = 0$, $Ro_t = 0$). Finally, for one of the seven oscillating scenarios (E), U_{tide} was approximately halved (E2) and doubled (E1) to investigate the effects of slower and faster tidal flow. For the purposes of this study, we further analysed cases Ek and D (comparison of a rotating but non-oscillating BBL with a rotating and oscillating BBL at the same geographical latitude) and cases E2, E and E1 (comparison of different tidal current-speed amplitudes for a given geographical latitude). In all eight main cases, the rotations of the tidal current vector occurred in the direction that would be expected from the direction of the Coriolis force (co-rotation): that is, both the free-stream tidal current and the Coriolis-related current rotated anticlockwise, with $f < 0$ and $\omega > 0$. The effects of counter-rotation of these two flow components will be discussed in Section 3.1.2 below.

2.3. Two methodological considerations

The sediment traps were deployed ~10 km to the south of the current-meter and transmissometer site. However, for the reasons given below, we think that any effects of the lack of exact co-location would have been sufficiently small for our interpretation of the results to be robust. On a space scale of only 10 km, there is no reason to believe that time-averaged far-field fluid dynamics would have been very different at the sites ('far field' relates to flow components that are controlled by processes in the interior ocean and not influenced by local interactions with the seafloor). However, the current-meter site was ~1.5 km (~2.5 km) to the SSE of the rise (summit) of a short abyssal hill whose summit area is ~200 m above the surrounding plain. Interactions of far-field flow components with a topographic obstacle can lead to local distortion of the flow field. Turnewitsch et al. (2013) showed that internal-tide generation is likely to occur in some localities on the hill. Barotropic tides and the residual flow may be deflected locally by the topography, but this deflection is likely to be comparatively weak and confined to the hill itself as the hill is short and mass-density stratification of the ambient water column is weak (see the exploration of the fluid-dynamic parameter space in Fig. 20 of Chapman and Haidvogel (1992) and in Figs. 2–4, 8, 15, 16 of Turnewitsch et al. (2013)). So, while *on the hill* there is likely to be a topographic influence on particle dynamics, *away from the hill* (beyond the rise line) fluid dynamics in near-seafloor waters should be very similar to the more distant far field. We, therefore, feel confident that the fluid dynamics in the trap and current-meter areas can be assumed to have been sufficiently similar for our interpretation to be valid.

The other point that needs to be addressed is whether lateral movement could have affected the trap-derived fluxes at different heights above the seafloor differentially. The residual near-seafloor currents in the study region were almost always towards northerly directions (Vangriesheim et al., 2001). That is, the traps were in the approximate upstream region of the current meter and transmissometer. It is unlikely that the current meter and transmissometer were on exactly the same streamline as the traps. But given the absence of any hill- or larger-scale topographic seafloor features between the traps and the current-meter sites, it seems safe to assume that the traps were passed by the same water *type* that then also passed the current meter and transmissometer. The short hill near the current-meter site was approximately *downstream* of the current-meter and trap sites and therefore unlikely to have introduced a vertical gradient in trap-derived fluxes. In addition, it needs to be noted that Turnewitsch et al. (2008) reported evidence for an advection signal in the vertical distribution of the nat-

urally occurring, short-lived particle tracer thorium-234 in the study region, with the signal most likely originating from flow/hill interactions in the *upstream* region further south. However, it was concluded that this was a 'fossil' signal and that larger, settling particle aggregates that were advected away from the upstream hills would have left the bottommost 100 s of meters of the water column by the time the upstream waters had reached our sampling sites. Overall, we can, therefore, be confident that lateral movement is unlikely to have impacted the trap-derived fluxes at different heights above the seafloor differentially.

3. Results and discussion

3.1. Physical-oceanographic aspects of the near-seafloor water column

3.1.1. Flow components

The deep residual flow in the study area at 15 mab was shown by Vangriesheim et al. (2001) to be directed towards northerly directions and, during their study, had an average current speed of ~2.8 cm s^{-1}. Every few months there was a change in the net current direction which occurs over time scales of days up to a few weeks. In terms of current speeds, low-frequency current components (periods >28 h) and semidiurnal oscillations are the strongest flow components (Fig. 2).

If the barotropic (surface) tide in mass-density-stratified water interacts with a topographic seafloor feature baroclinic (internal) tides form. If the tidal frequency is higher than the local inertial (Coriolis) frequency ($\omega > f$) the generated internal tide can propagate away from the generation site as an internal wave at tidal frequency; otherwise it remains trapped at the generation site. For diurnal and semidiurnal tides, the critical latitudes are ~30° and ~74.5°. That is, diurnal internal tides that form in the study area can be expected to remain trapped at their generation sites; by contrast, semidiurnal internal tides can propagate. Hence, there may be baroclinic tidal components in the semidiurnal oscillations of the measured currents. These propagating semidiurnal baroclinic tides are the most likely reason (a) for the deviation of the measured semidiurnal tidal ellipse from the ellipse of the barotropic tide as predicted by the TPXO model (Egbert and Erofeeva, 2002) (Fig. 3a–c), and (b) for the lack of a continuously clear neap/spring signal in the measured tidal (semidiurnal + diurnal) current-speed time series (3d,e) and the absence of a clear neap/spring signal in the time series of total current speeds (Fig. 8).

Interestingly, the measured neap-tide current ellipse was generally narrower in the E-W direction compared to the measured spring-tide current ellipse (Fig. 4a and b). This finding for the overall dataset also applied to the time interval in July 1997 during which the thickness of the BML was determined (Fig. 4c and d). At a given geographical latitude, the circularity of an ellipse is indicative of the relative importance of flow components that differ in their rotational behaviour. Rotational behaviour of different flow components, in turn, influences BBL properties such as turbulence intensities and BBL thicknesses. Before moving on to particle and biogeochemical BBL dynamics, we will, therefore, briefly review and discuss pertinent aspects of co- and counter-rotating flow components in BBLs.

3.1.2. Co- and counter-rotating flow components

Effects of co- and counter-rotation on BBL thickness --- For a non-oscillating ('steady') but rotating boundary layer, the Ekman-layer thickness h_{Es} can be approximated by $h_{Es} = (2K/|f|)^{0.5}$, where K is eddy (and not kinematic) viscosity (Munk et al., 1970; Weatherly et al., 1980). By contrast, for an oscillating *and* rotating boundary layer, Ekman-layer thickness $h_{E\pm}$ would be approximated by $h_{E\pm} = (2K/|\pm\omega + f|)^{0.5}$. Whether ω is positive or negative depends on whether it is counter-clockwise ($+\omega$) or clockwise ($-\omega$) polarized relative to f which is >0 and <0 for clockwise (northern hemisphere) and counter-clockwise (southern hemisphere) rotation, respectively. Consequently, in comparison to a non-oscillating Ekman layer, the respective implications for the Ekman-layer thickness are a thickening for co-rotation (scenarios $h_{E-+} = (2K/|-\omega + f|)^{0.5}$ and $h_{E+-} = (2K/|\omega - f|)^{0.5}$), with a theoretically infinitely thick Ekman layer if $-\omega + f = 0$ or $\omega - f = 0$, and a thinning for counter-rotation (scenarios $h_{E++} = (2K/|\omega + f|)^{0.5}$ and $h_{E--} = (2K/|-\omega - f|)^{0.5}$).

For the more recent study of Sakamoto and Akitomo (2009), two key scenarios (their cases Ek and D: see Section 2.2) can be compared at a single given f (geographical latitude), with the scenarios differing in their rotational properties (Fig. 5): (1) a non-oscillating Ekman layer (case Ek); and (2) an oscillating Ekman layer where the current vector rotates in the same direction as in the non-oscillating case, i.e., where co-rotation occurs (case D). At a temporal Rossby number of $Ro_t = |\omega/f| = 1.05$, the two scenarios can be interpreted in terms of ω values for a diurnal and a semidiurnal tide: for a diurnal tide, $Ro_t = 1.05$ would correspond to a geographical latitude of 28°, whereas for a semidiurnal tide, it would correspond to 72°. It turned out that the boundary layer in case D was almost 14 times thicker than in case Ek. Although an explicit model run for a counter-rotating scenario was not carried out by Sakamoto and Akitomo (2009), it was speculated that the boundary layer in case D could be more than 40 times thicker than in the counter-rotating case (and it would seem that the boundary layer in the counter-rotating case would then be ~3 times thinner than in the pure Ek case) (Fig. 5a). For a given tidal current-speed amplitude, co-rotation almost always leads to a thickening of the BBL compared to a corresponding non-oscillating Ekman layer (exceptions occur near/at the equator for semidiurnal and diurnal oscillations; Sakamoto and Akitomo, 2009). It is very important to note that these very significant differences in boundary-layer thickness occur for the same tidal current-speed amplitude and are entirely dependent on the effects of the rotational behaviour of the boundary layer on turbulence intensities within the boundary layer.

Effects of tidal oscillation on turbulence in the BBL --- For weakly mass-density-stratified boundary layers that oscillate at the low current speeds that are typical for most areas of the deep seas, it has been shown that, in comparison to the steady-state law-of-the-wall situation, even relatively long oscillation periods of many hours can significantly change the form of the near-bottom current-speed profiles as well as the dynamics of the rate of turbulent energy dissipation (Lorke et al., 2002). In this context, the study of Sakamoto and Akitomo (2009) showed that a key effect of co-rotational tidal oscillation is a significant increase of absolute turbulence intensities across a very large part of the *upper* BBL (i.e., above the log layer), leading to the aforementioned thickening of the BBL and BML (Fig. 5b and c). By contrast, closer inspection of the waters *in close vicinity to the seafloor* in the aforementioned cases Ek and D of Sakamoto and Akitomo (2009) revealed not only reduced absolute current speeds and vertical current-speed gradients (Fig. 5a), but also reduced absolute turbulence intensities (Fig. 5b) due to the effects of tidal oscillations. That is, while co-rotational oscillation increases average turbulence intensities in the upper BBL, it decreases turbulence intensities near the seafloor.

Effects of tidal oscillation on boundary shear stress --- As outlined in Section 1, near-seafloor particle dynamics in the deep sea are partly driven by rebound and/or even resuspension. Within this context, it is, therefore, also important to note that Weatherly et al. (1980) related different combinations of co- and counter-rotation to effects on the average 'boundary shear stress', τ_0, at the seafloor. For a quasi-steady (geostrophic) background flow of current speed G and constant K, the boundary shear stress can be

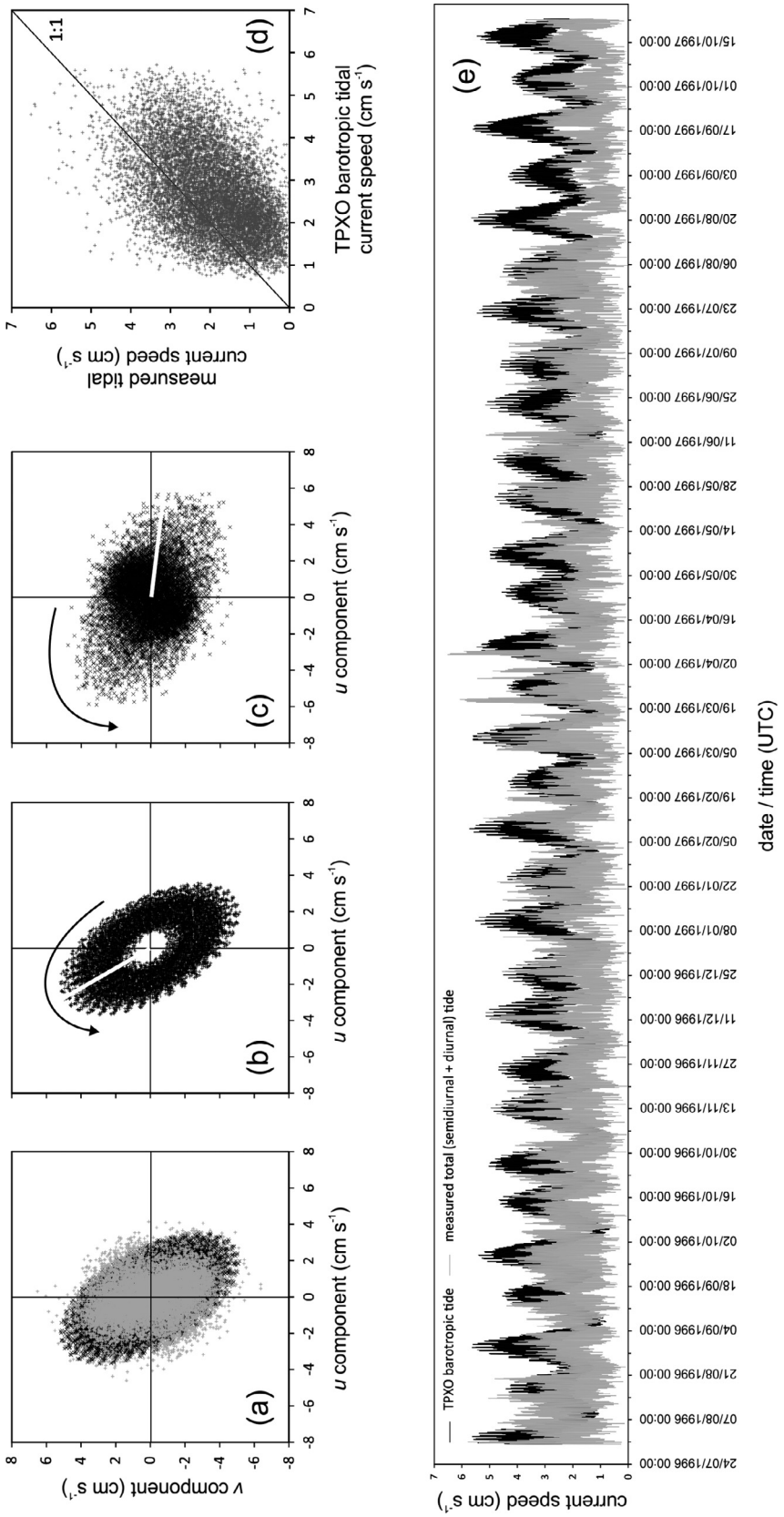

Fig. 3. (a) Comparison of the TPXO barotropic tidal currents (black symbols) with measured currents (grey symbols) in tidal period bands. (b) Only the barotropic TPXO results are shown. (c) Difference between the barotropic TPXO tide and the measured currents. Arrows in (b) and (c) indicate prevalent counterclockwise rotation of the current vector. White lines in (b) and (c) indicate the same point in time. (d) Comparison of TPXO barotropic tide current speeds and measured total (semidiurnal + diurnal) tidal current speeds. (e) Same as (d) but as a time series. (a–e) The barotropic data are derived from the TPXO model (Egbert and Erofeeva, 2002) for the time interval between 30 July 1996, 08:00 UTC, and 22 October 1997, 11:00 UTC, at hourly resolution. The measured tide is the combination of semidiurnal (10–15 h) and diurnal (21–28 h) bands from the measured data set of Vangriesheim et al. (2001) at the same hourly resolution as the TPXO data.

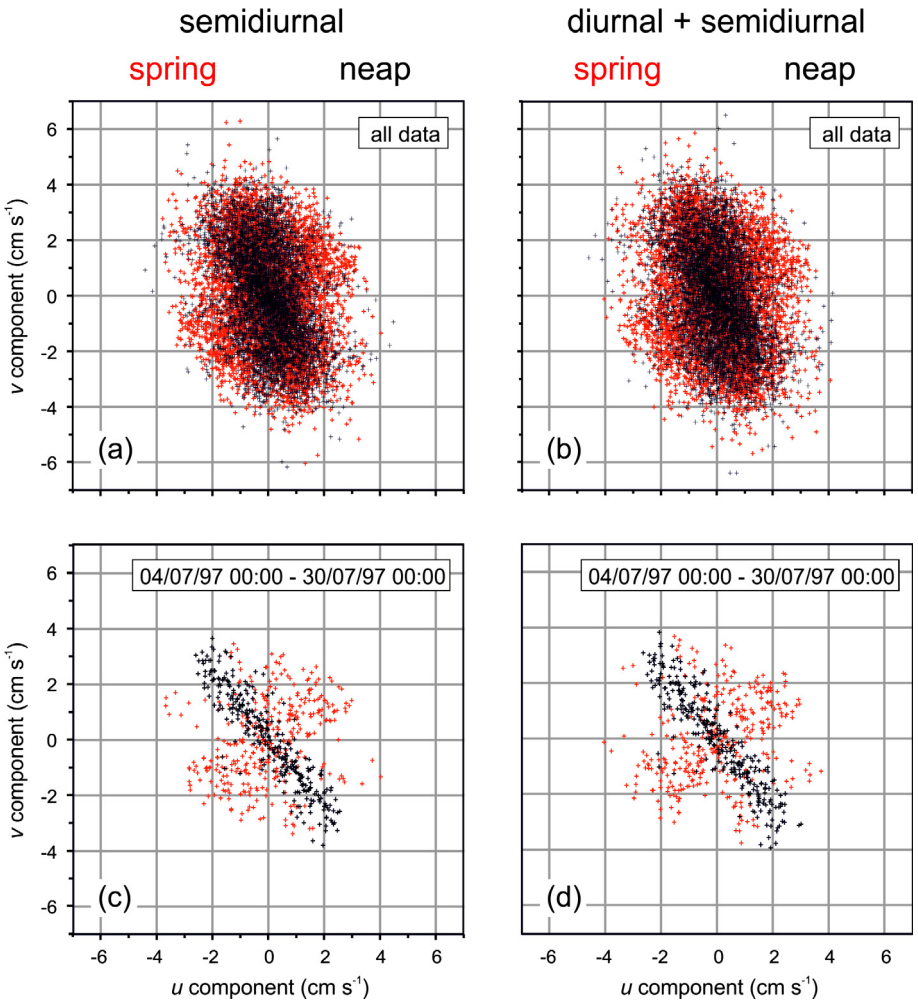

Fig. 4. (a) Semidiurnal band (10–15 h) currents during spring tide (red symbols) and neap tide (black symbols). (b) Total (semidiurnal band + diurnal band) currents during spring tide (red symbols) and neap tide (black symbols). (a) and (b): Extracted from data between 30 July 1996, 08:00 UTC, and 22 October 1997, 11:00 UTC, at hourly resolution, measured by Vangriesheim et al. (2001) at 15 mab. (c) and (d): same as (a) and (b), respectively, but only for the time interval in July 1997 for which the time series of BML thicknesses was obtained (Fig. 6a). A given neap-tide interval was defined by the time boundary half-way between the peak of the previous spring tide and the trough of the current neap tide, and by the time boundary half-way between the trough of the current neap tide and the peak of the following spring tide. A spring-tide interval was defined in an analogous way. (For interpretation of the references to colour in this figure legend, the reader is referred to the web version of this article.)

approximated by $\tau_{0s} = G\,(|f|K/2)^{0.5}$. Moreover, for co-rotation, the respective relations would be $\tau_{0-+} = G/2\,(|-\omega + f|K/2)^{0.5}$ and $\tau_{0+-} = G/2\,(|\omega - f|K/2)^{0.5}$, and for counter-rotation, $\tau_{0++} = G/2\,(|\omega + f|K/2)^{0.5}$, and $\tau_{0--} = G/2\,(|-\omega - f|K/2)^{0.5}$. That is, in comparison to a non-oscillating Ekman layer, both co- and counter-rotation lead to a reduction of τ_0, but for co-rotation the reduction is larger than for counter-rotation (Fig. 6).

Further analyses of the aforementioned, more recent data sets of Sakamoto and Akitomo (2009) confirm that, in comparison to a rotating and non-oscillating boundary layer, a combination of rotation and oscillation leads to temporally oscillating boundary shear stress whose instantaneous values are always lower than in the purely rotating case (see example in the insert of Fig. 5).

However, the *range* of instantaneous turbulence intensities in the immediate vicinity of the boundary (in the buffer layer (BL) and viscous sublayer (VSL)) is higher in the aforementioned case D than in case Ek of Sakamoto and Akitomo (2009) (Fig. 5b and c). This is important because the log-normal and positively skewed probability density functions of the statistical distribution of bed shear stresses (e.g., Cheng and Law, 2003) indicate that this wider range of near-boundary turbulence intensities implies an increased probability of very rare but also very high instantaneous boundary shear stresses in the co-rotational scenario. That is, at a given current-speed amplitude, co-rotational tidal oscillation in a rotational frame reduces average boundary shear stress, but increases the probability of rare events of very high bed shear stress.

Effects of current-speed amplitude --- At a given f and ω, the current-velocity amplitude of the oscillating flow component also influences BBL dynamics. An example from the datasets of Sakamoto and Akitomo (2009) is shown in Fig. 7 for co-rotation at $Ro_t = |\omega/f| = 1.2$. This case can also be interpreted in terms of ω values for a diurnal tide (geographical latitude: 24.5) and a semidiurnal tide (geographical latitude: 56°). Three different current-speed amplitudes for the oscillatory flow component in the free-stream flow were considered: 4.3 cm s^{-1} (case E2), 8.5 cm s^{-1} (case E) and 17.1 cm s^{-1} (case E1). With increasing current-speed amplitude, the BBL thickens (Fig. 7a and b) and the peak in turbulence intensity in the BL moves closer to the boundary (Fig. 7b). With increasing speed amplitude, overall turbulence intensities and boundary shear stresses also increase (Fig. 7a–e).

Implications for the PAP study area --- As the PAP area is on the northern hemisphere ($f > 0$) and the local barotropic tide rotates counterclockwise ($\omega > 0$), there is counter-rotation that is expected to lead to a comparatively thin Ekman layer. Here, we make the assumption that Ekman-layer and BML thicknesses are approximately equal or are at least related to each other. In

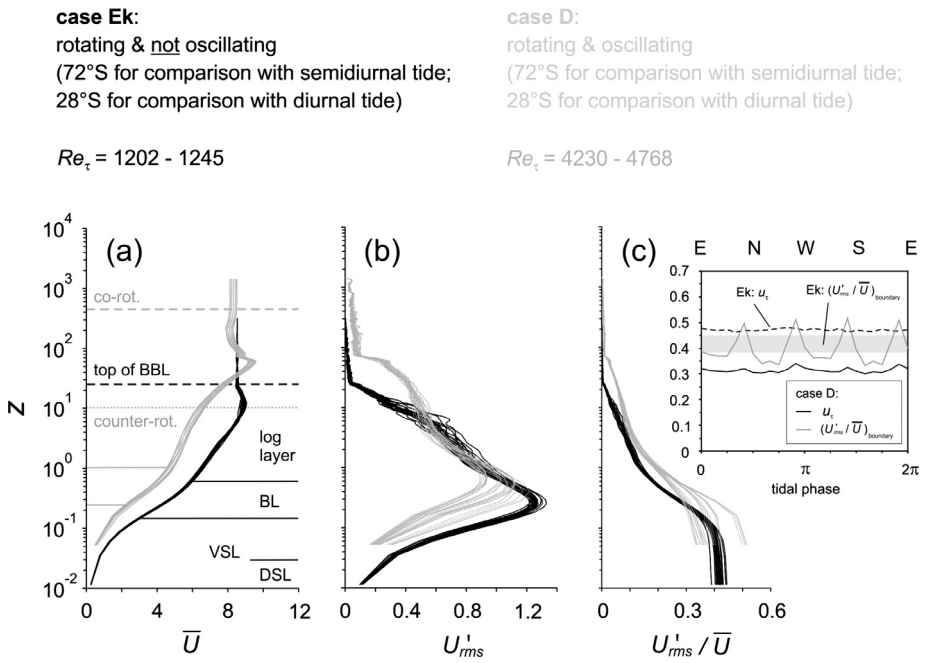

Fig. 5. Comparison of a numerically modelled rotating, non-oscillating BBL (black: case Ek) with a rotating, semi-diurnally oscillating, anticlockwise-polarised (Coriolis parameter $f < 0$, tidal frequency $\omega > 0$) BBL (grey: case D) at a geographical latitude of 72°S. The former case does not differ significantly from a steady non-rotating, non-oscillating BBL. In both cases Ek and D the free-stream current speed of the forcing flow is the same. z is distance from the seafloor. For each case, 26 temporally equidistant graphs are plotted, capturing the duration of one semidiurnal tidal cycle. (a) Average current-speed, $\overline{U}$; grey dashed line: top of BBL for co-rotating case D; grey dotted line: speculative top of BBL for counter-rotating case D. (b) Turbulence intensity expressed as root-mean-square (rms) of current-speed fluctuations, U'_{rms}. (c) Turbulence intensity expressed as $\overline{U}/U'_{rms}$. Abscissae and ordinates in relative units. $Re_\tau = \delta u_\tau / \nu$, where δ is the BBL thickness, u_τ is the shear velocity at the boundary, and ν is kinematic viscosity of the seawater. Inset: time series of one semidiurnal tidal cycle of u_τ for case Ek (dashed line) and case D (solid black line) and of $\overline{U}/U'_{rms}$ in case Ek (grey area) and D (grey solid line).

our study, during the 18-day time series in July 1997, BML thicknesses could be determined from vertically largely invariable transmissometry values near the seafloor (see Fig. 3a of Turnewitsch and Springer, 2001). Over the 18 days, BML thicknesses varied between a minimum of ~25 m during neap tide and a maximum of ~63 m during spring tide (Fig. 6). Given the above overview of BBL fluid dynamics, increased BML thicknesses during spring tides could be expected to occur because of an overall tendency towards higher current speeds that normally lead to thicker boundary layers (Fig. 7). However, as mentioned above, in the PAP area, neither total nor tidal (semidiurnal + diurnal) measured current speeds displayed continuously clear neap/spring oscillations (Figs. 3 and 8). So, while neap/spring current-speed oscillations may play a role in controlling BBL fluid dynamics, they are unlikely to have been the sole or main factor at the PAP sites.

However, as described in Section 3.1.1, there was a difference in the rotational behaviour of the currents at 15 mab between neap and spring tides: during spring tides, the measured tidal ellipse was more *circular* and mostly rotating counterclockwise, indicating the strong predominance of flow components that co-rotate counterclockwise; by contrast, during neap tides, the measured tidal ellipse was more *elongated*, indicating significant contributions of both clockwise- and counterclockwise-rotating tidal flow components (Fig. 4). If co-rotating flow-components are not strongly out of phase, their co-rotation should lead to Ekman-layer (BML) thickening, whereas their counter-rotation should contribute to Ekman-layer (BML) thinning. That is, during spring tides in the PAP area, the Ekman layer (BML) should have been thicker than during neap tides, even though tidal current-speed amplitudes were similar; and this is what was observed (Figs. 4 and 6). In addition, during neap tides, the *relative* importance of the clockwise-rotating near-inertial oscillations also increased (cf. Fig. 2d), contributing to the strength of overall counter-rotation of flow components and, as a consequence, to further Ekman-layer (BML) thinning during neap tides.

Given the rotational behaviour of the flow components in the PAP area, there should have been three main effects of neap/spring oscillations. (1) Neap/spring fluctuations of Ekman-layer and BML thicknesses and associated turbulence intensities in the BBL should have been particularly high (see top of Fig. 6), with reduced (increased) BML thicknesses and turbulence intensities during neap (spring) tides. (2) Neap/spring fluctuations of the boundary-layer stress τ_0 should have been particularly low (see top of Fig. 6). (3) And, as a consequence, neap/spring variability of BBL fluid dynamics should have had a higher impact on particle dynamics *within* the BBL and a lower impact on particle dynamics right at the SWI.

3.2. Influence of BBL dynamics on fine-grained material

The time series of nephelometer readings at 1 mab and current velocities at 15 mab (Vangriesheim et al., 2001) were compared with output from the barotropic TPXO tide model for the respective time intervals (Fig. 8) as this gives a clear indication of the timing and magnitude of semidiurnal as well as neap-spring tidal oscillations of the local barotropic tide. The purely barotropic tidal current speeds are generally weaker than the measured total current speeds. However, despite the generally higher current speeds of the total flow, the turbidity time series does not show a close relation with total current speeds on time scales of days to weeks. By contrast, it displays evidence for an effect of the neap/spring tidal forcing as reflected in the barotropic tidal oscillations: nephelometer readings at 1 mab are often higher during neap tides and/or during the early stages of acceleration into a spring tide (Fig. 8). This trend tends to be clearer when the turbidity is generally

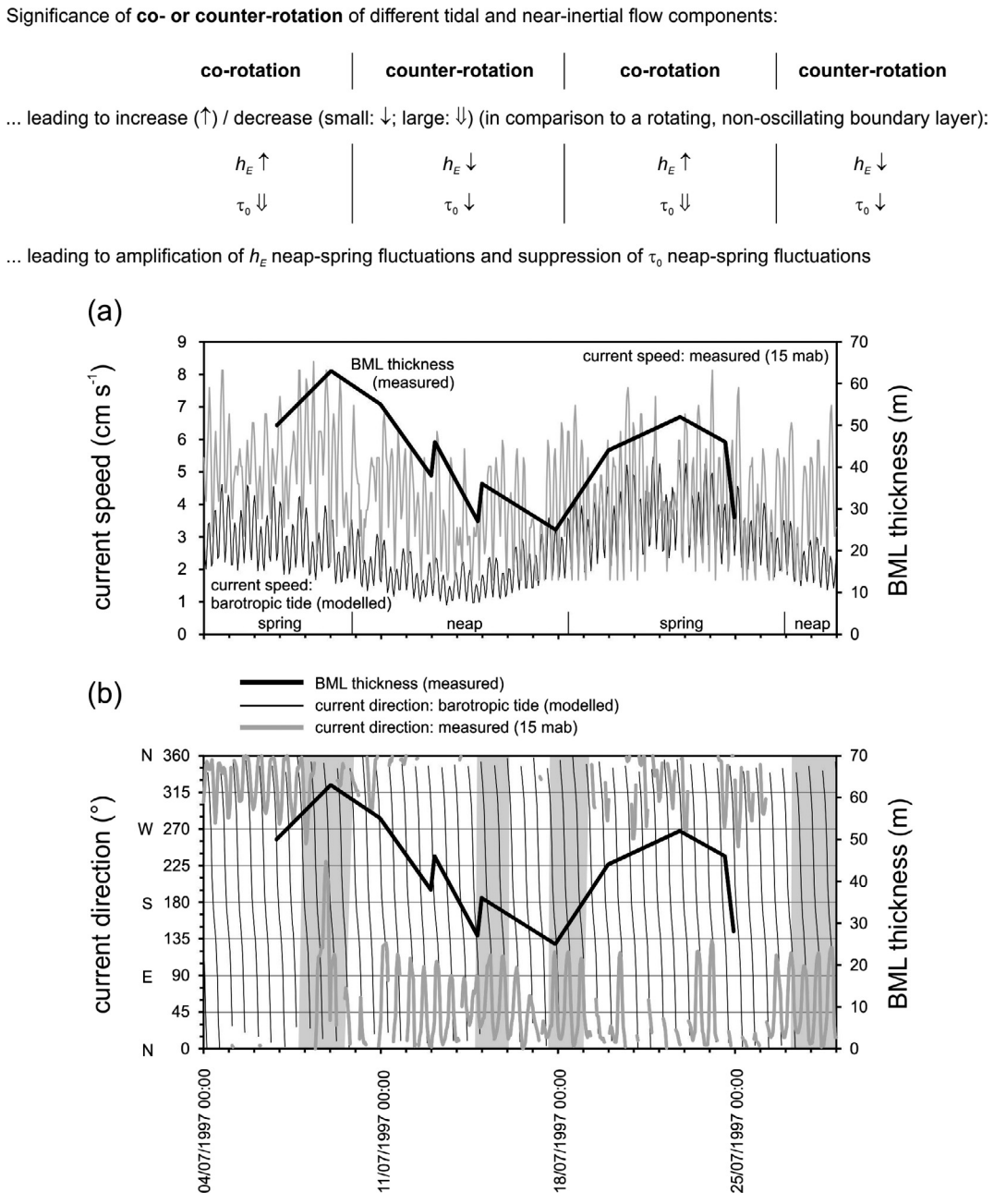

Fig. 6. Example of variability of currents and BML thickness in the study region. Measured BML thickness plotted with (a) modelled TPXO barotropic tidal current speeds and measured current speeds at 15 mab; and with (b) modelled barotropic tidal current directions and measured current directions at 15 mab. The grey areas in (b) indicate time intervals when the total tidal (semidiurnal + diurnal) current vector was undergoing at least two consecutive clockwise rotations. This happened during transition from a spring into a neap tide and during neap tides. Above the plots, the predominance of co- or counter-rotation of tidal flow components near the seafloor is indicated. The theoretically and numerically derived effects (increase vs. decrease relative to a rotating but non-oscillating boundary layer) on Ekman-layer thickness (h_E) and boundary shear stress (τ_0) and the resulting effects (amplification vs. suppression) on neap/spring fluctuations of h_E and τ_0 are also shown.

increased (probably as a consequence of varying primary fluxes from the surface and interior ocean). The finding that, on the time scale of neap/spring tidal cycles, turbidity levels near the seafloor are more closely related to the generally lower barotropic tidal current speeds than to the generally higher total current speeds suggests that there are other factors in addition to current speed that influence particle dynamics in near-seafloor waters (Turnewitsch et al., 2013). Given the considerations in Section 3.1.2, the additional factors seem likely to involve the turbulence specifics of oscillating and rotating BBLs and temporal (neap/spring) variability of the oscillating forcing-flow components (with some modulation due to other flow components).

This notion is corroborated by the studies of Pak (1983), Vangriesheim and Khripounoff (1990), Auffret et al. (1994), Vangriesheim et al. (2001) and Turnewitsch et al. (unpublished data from the Cape Verde Rise) who showed that on the shorter semidiurnal time scale current-velocity oscillations can be reflected in turbidity oscillations near the seafloor (on the order of 0.1–1 mab) at surprisingly low current speeds of only a few centimeters per second, i.e., at current speeds that are too low to drive rebound or even resuspension. This also supports the earlier conclusion that neap/spring variability of fluid dynamics *within* the BBL is more important in controlling particle dynamics than neap/spring variability of processes at the SWI.

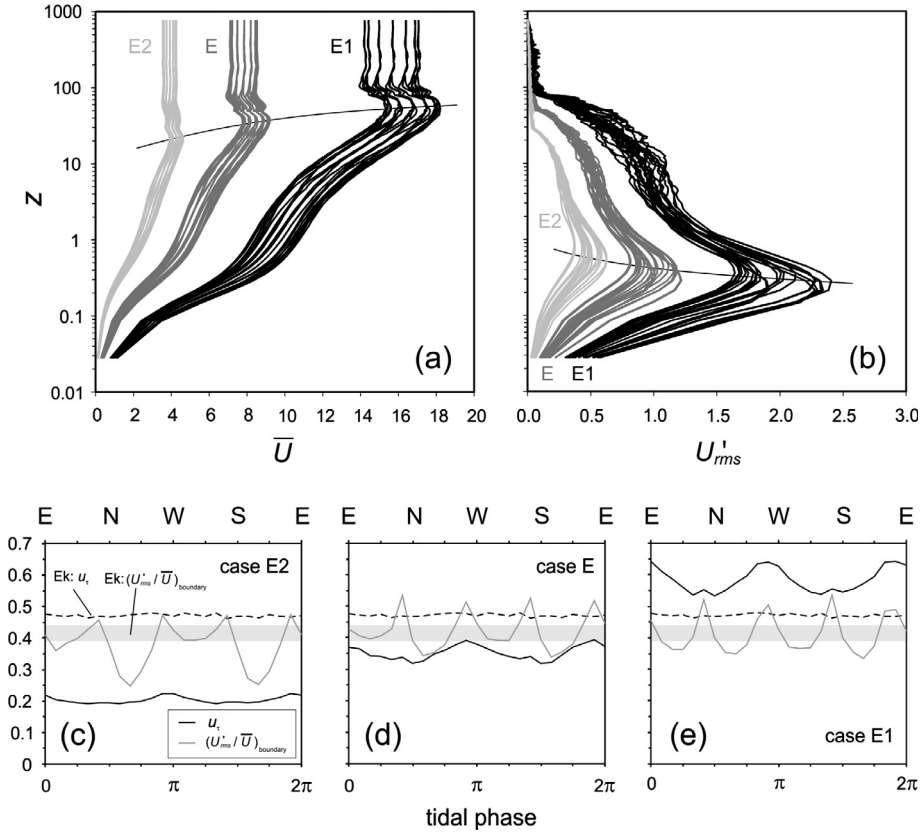

Fig. 7. Effects of increasing tidal current-speed amplitude (case E2 < case E < case E1) on BBL properties (all values are plotted on relative scales). (a) Profiles of average current-speed, $\overline{U}$, for the three different cases, with the maximum free-stream current speed of cases E and E1 being larger by a factor of ~2 and ~4, respectively, than the maximum free-stream current speed of case E2. (b) Corresponding profiles for the root-mean-square of current-speed fluctuations, U'_{rms}. In (a) and (b), for each case, 26 temporally equidistant graphs capturing the duration of one semidiurnal tidal cycle are plotted. The thin solid lines running across and between the case profiles are drawn by hand and illustrate the thickening of the BBL (in (a)) and the increasing proximity to the boundary of the turbulence peak (in (b)) with increasing tidal current-speed amplitude. (c) and (d) Same as inset in Fig. 5, but for cases E2 (c), E (d) and E1 (e).

An important resulting question now is whether the fluid-dynamic neap/spring oscillations that influence dynamics of fine-grained particles around 1 mab (and probably in other parts of the BBL) also translate into dynamics of larger aggregated, settling particles and biogeochemical fluxes within the near-seafloor water column.

3.3. Arrival of settling particles from a surface-ocean bloom

The sediment-trap study captured the peak current speeds of four barotropic TPXO spring tides and the minimum current speeds of three barotropic TPXO neap tides (Fig. 9). Peak current speeds of the first two spring tides and minimum current speeds of the first neap tide coincided very closely with the mid-points of the first three sediment-trap sampling intervals. Afterwards, there is a rising offset, with the sampling-interval mid-points increasingly lagging the alternating barotropic current-speed spring peaks and neap minima. The maximum lag at the end of the sampled time series is ~3 d (Fig. 9). Despite this increasing offset, it can be concluded that the trapping intervals were reasonably well in phase with the neap/spring barotropic tidal oscillations.

Another advantage of this study is that it captured the arrival of sedimenting material that originated from a plankton bloom in the surface ocean. Hence, the study can aim to assess the extent of the influence of neap/spring tidal cycles on biogeochemical fluxes in the near-seafloor waters for a range of primary-flux magnitudes.

Overall, absolute downward fluxes of the main biogeochemical particle constituents PIC, BSi, POC and PN at all three sampled heights above the seafloor show significant increases from the beginning to the end of the deployment periods (Fig. 9a–d). LM also shows an overall flux increase at all three heights (Fig. 9e), but there is a major difference in the shape of the temporal increase between 569 mab on the one hand and 2 mab and 40 mab on the other hand; and the LM flux increases generally behave quite differently compared to the flux evolutions of the other main flux constituents. All the main flux constituents combine to lead to an overall rise of the downward mass flux of TPM (Fig. 9f).

When, for a given particle component, the flux time series are compared between different heights above the seafloor it is revealed that there are three types of components: PIC, LM and the other components. The organic main components (POC, PN) and BSi show an almost exponential flux increase at all three heights above the seafloor. By contrast, LM fluxes at 2 mab and 40 mab on the one hand and at 569 mab on the other hand diverge very strongly with the unfolding arrival of the settling bloom: within the bottommost tens of meters, the LM flux displayed an overall increase throughout whereas the lithogenic flux at 569 mab rose very slightly; only in the last week of the deployment period a very substantial and abrupt increase of the LM flux was recorded at 569 mab. This substantial divergence between POC, PN and BSi on the one hand and LM on the other hand that occurred over the first 5–6 weeks of the deployment period is most likely due to progressive accumulation of phytodetrital aggregates in the boundary layer, where these aggregates are recirculating and rebounding from the seafloor where these comparatively sticky

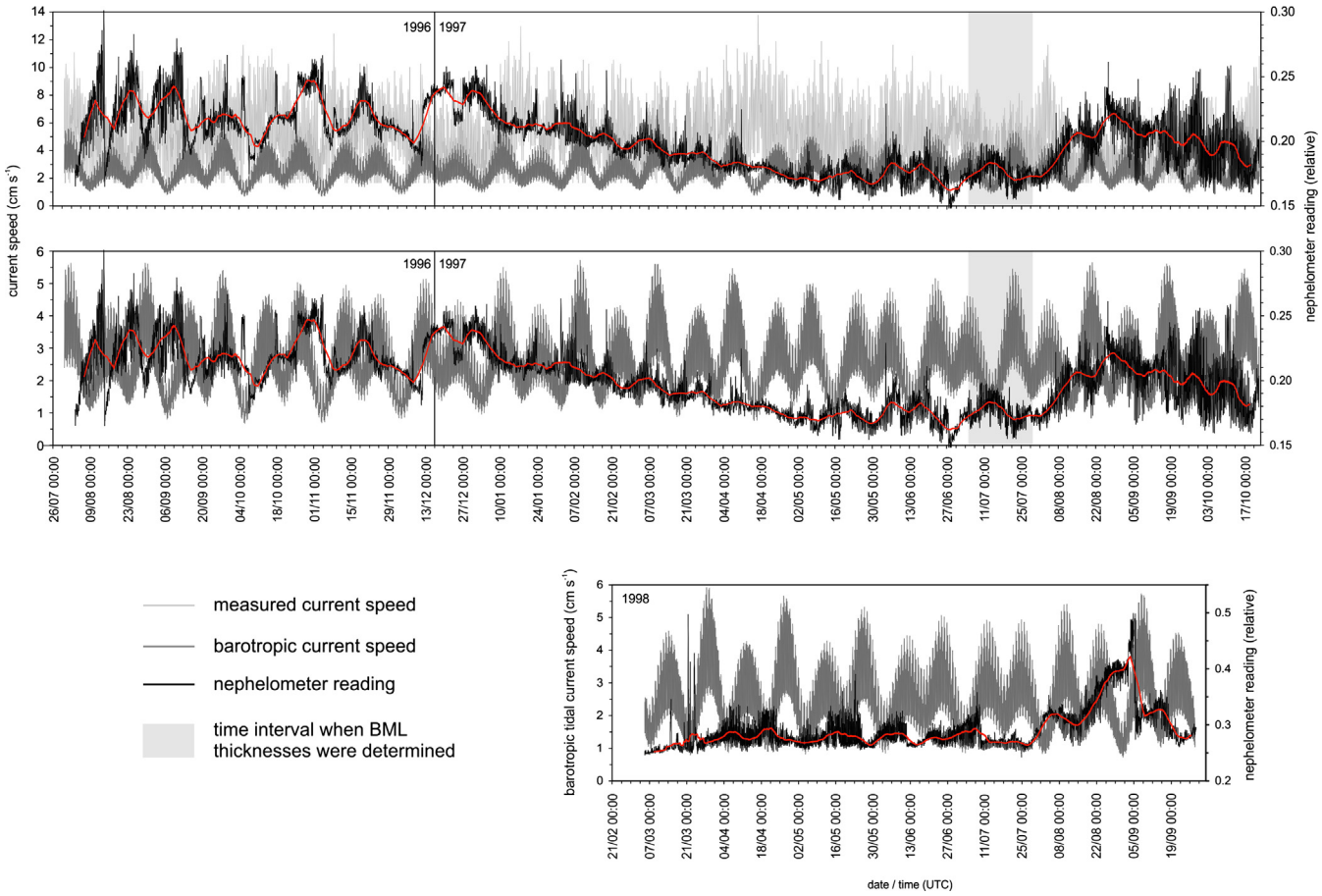

Fig. 8. (Top) Comparison of measured time series of nephelometer (relative-turbidity) readings from 1 mab with time series of measured current speeds at 15 mab (data from 1996/97; Vangriesheim et al., 2001) and corresponding barotropic tidal current speeds as derived from the barotropic TPXO tide model of Egbert and Erofeeva (2002). (Centre) Same as Top, but without the measured current speeds to show more clearly the relation between neap/spring cycles and turbidity. (Bottom) Same as Centre plot but for the time series from 1998 (there are no measured current speeds for the 1998 time window; nephelometer data from Vangriesheim et al., 2001). Red lines: smoothed nephelometer readings. The grey areas in the upper two plots indicate the time interval when BML thicknesses were determined on twelve occasions (see Fig. 6). (For interpretation of the references to colour in this figure legend, the reader is referred to the web version of this article.)

aggregates (Passow, 2002) might also 'pick up' older sediment particles from the SWI.

The reason(s) for the large, abrupt LM flux increase at 569 mab during the last sampling interval is (are) unclear. Local rebound and/or resuspension loops are unlikely to reach that high into the water column on such short time scales (Lampitt, 1985). It seems more probable that the composition of the primary flux had changed.

Finally, PIC appears to show a flux behaviour that is intermediate between LM on the one hand and POC, PN and BSi on the other hand, suggesting the influence of both primary-flux and rebound and/or RB&RS particles. A significant and quasi-continuous influence of rebound and/or RB&RS particles on near-seafloor settling fluxes of PIC in the Northeast Atlantic was also reported by Lampitt et al. (2000).

PIC/BSi, LM/POC, POC/BSi ratios and $\delta^{15}N$ signatures of the settling material displayed an overall decrease while POC/PIC ratios displayed an overall increase over the sampling period (Fig. 10). These trends indicate an increasing relative importance of opaline, organic-rich and 'fresh' particles with the unfolding arrival of the settling bloom. (POC/PN ratios displayed a slight decrease at 569 mab, but no clear trends at 2 and 40 mab.)

There are also differences between the BML-affected water layers (2 mab and 40 mab) on the one hand and 569 mab on the other hand. If the time series of $\delta^{15}N$, PIC/BSi, LM/POC and POC/BSi are compared between different heights above the seafloor it turns out that all these parameters are increased in the bottommost tens of meters of the water column while POC/PIC ratios are typically decreased. These differences most likely reflect the presence of older sediment particles (as indicated by higher $\delta^{15}N$, reduced BSi contents and increased LM contents) that are still involved in the rebound and/or RB&RS loops.

Fluxes of total hydrolysable amino acids (AA) and of hexosamines (HA) increased significantly throughout the sampling period at all three sampled heights above the seafloor (Fig. 11a and b). For AA, there is some evidence to suggest a flux increase within the bottommost tens of meters of the water column as compared to 569 mab. This increase towards the seafloor was less clear for HA, and, for both AA and HA, it disappears at the highest overall fluxes during the last week of the deployment period.

At 2 mab and 40 mab there was no strong evidence for a temporal change of the AA- and HA-bound carbon (Fig. 11c and e) and nitrogen (Fig. 11d and f) fractions of total POC and total PN. At 569 mab there may have been an overall increase of the carbon fractions and, to a lesser degree, possibly also the nitrogen fraction, also indicating the arrival of fresher material. But scatter of the data was significant.

A core interest of this paper is the effect of an abyssal BBL on biogeochemical constituents of particle aggregates as they settle from the interior ocean into, and recirculate within, the BBL. The flux time series has three properties that help address this core

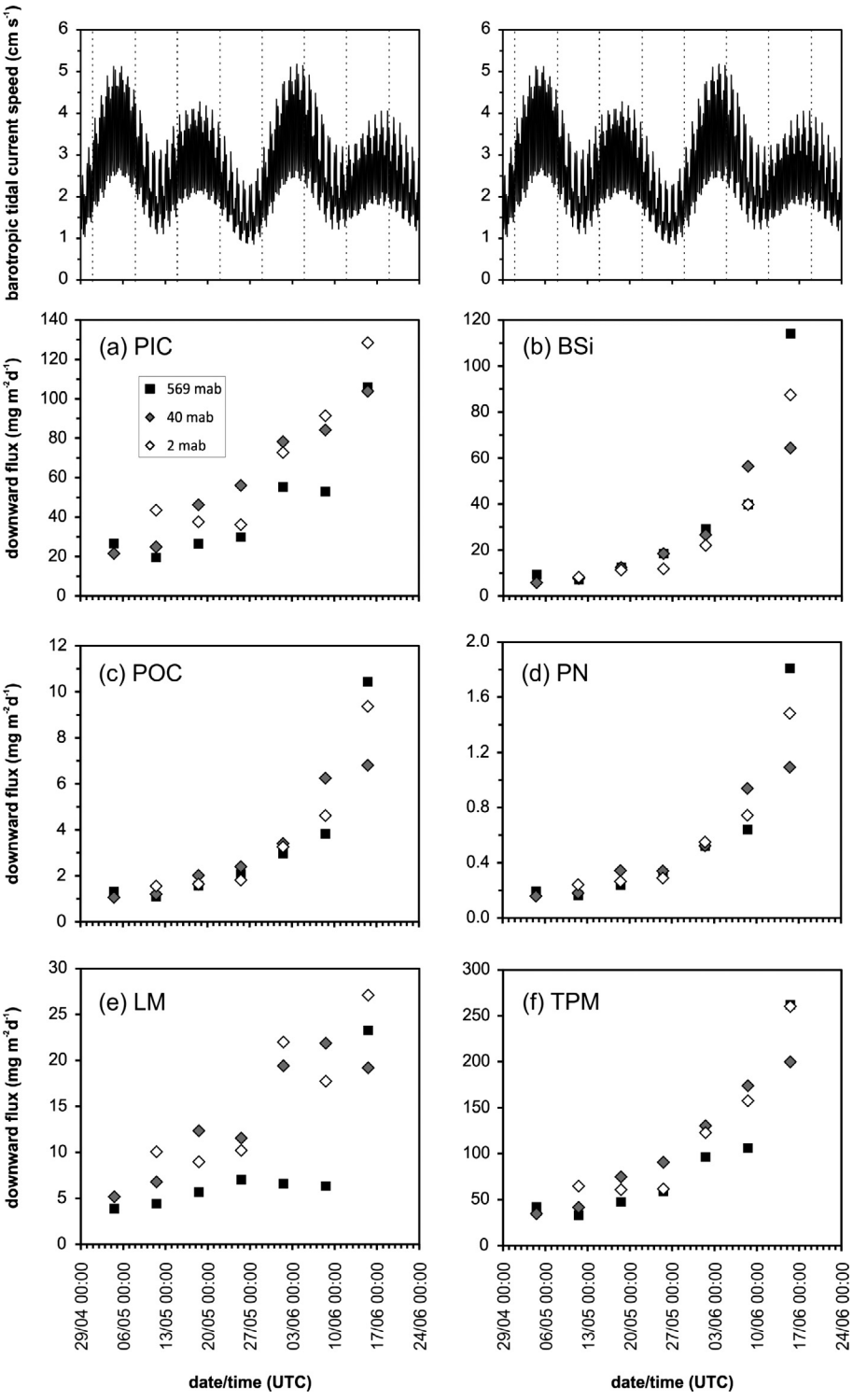

Fig. 9. Time series of the downward flux at 2, 40 and 569 mab of (a) particulate inorganic carbon (PIC), (b) biogenic silica (BSi), (c) particulate organic carbon (POC), (d) particulate nitrogen (PN), (e) lithogenic material (LM), and (f) total particulate matter (TPM). Above each plot column, a time series of TPXO barotropic tidal current speeds for the sediment-trap sampling period is shown to indicate the timing of the neap/spring tidal cycles. Vertical dashed lines indicate the start/end of trap sampling intervals.

interest. (1) A notable advantage of this dataset is that it captures time just before and during the arrival of a pulse of fresh material from the surface ocean, with an interval of increasing primary fluxes. This non-steady-state situation can be exploited to reveal information on the behaviour and fate of settling material in the near-seafloor water column. (2) The time series captures several neap-spring tidal cycles, with sample intervals approximately centred around the mid points of neap and spring tides. The samples should, therefore, constitute integrative biogeochemical signals due to neap and spring tides. (3) Of the main constituents of the settling material only LM can be safely assumed to be chemically inert on the time scales of plankton blooms and neap-spring tidal cycles. This is a great advantage as LM dynamics can then be used to investigate transport-only processes in the BBL: it can be assumed that the LM results reflect the net effect of processes such as particle settling, deposition, rebounding and resuspension, and

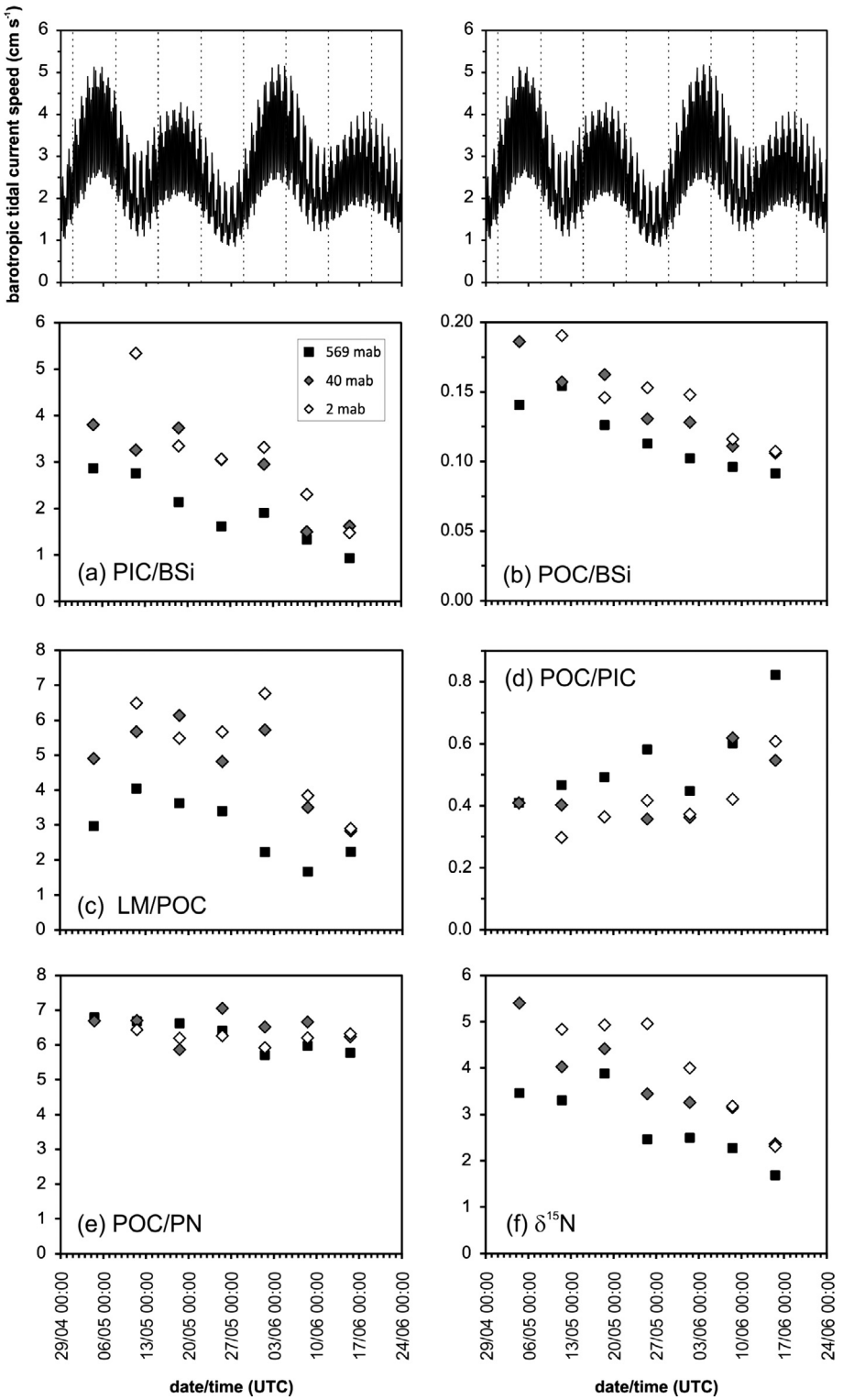

Fig. 10. Same as Fig. 9, but for the weight-% ratios of (a) PIC/BSi, (b) POC/BSi, (c) LM/POC, (d) POC/PIC and (e) POC/PN, and for (f) $\delta^{15}N$.

aggregation and disaggregation. As a consequence, deviations of the behaviour of the biogeochemical constituents from the behaviour of LM could, in principle, then be used to assess BBL effects on biogeochemically relevant processes other than transport: i.e., release (uptake) of organic material from the particulate (dissolved) into the dissolved (particulate) phase through leaching of organic matter and/or organic-matter remineralisation (adsorption and/or biomass production); and dissolution of biominerals (here: calcite, biogenic silica).

3.4. Effects of neap/spring tidal cycles on near-seafloor biogeochemical fluxes?

3.4.1. Observations

A fraction of the particles that were biologically produced in the surface ocean settles into the deeper water column. Most of the biogeochemical decomposition of these settling particles takes place within the topmost hundreds of meters. On typical time scales of a few weeks that it takes the particles to settle from water

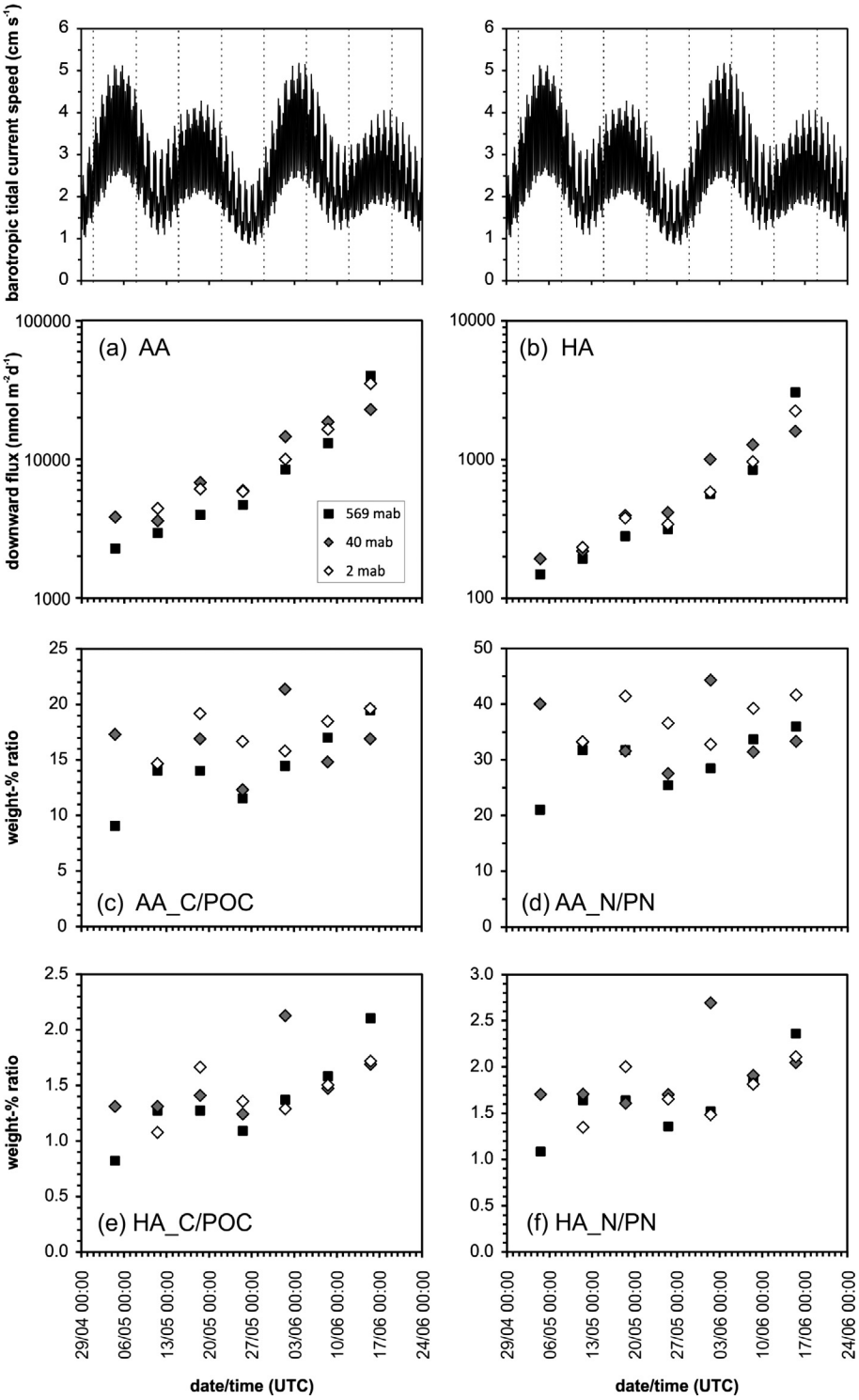

Fig. 11. Same as Fig. 9, but for downward fluxes of (a) total hydrolysable amino acids (AA) and (b) hexosamines (HA), and for weight-% ratios of (c) AA carbon and POC, (d) AA nitrogen and PN, (e) HA carbon and POC, and (f) HA nitrogen and PN.

depths of ~1000–1500 m into the abyssal near-seafloor water column, comparatively little additional net biogeochemical particle decomposition takes place. We, therefore, assume that there is negligible particle degradation between the 569 mab trap and the top of the BML or BBL.

When the settling particles enter the BML they are exposed to very different fluid dynamics as compared to the deep interior ocean and are eventually 'stopped' at the SWI. The macroscopic appearance of the trap-collected particles indicated that phytodetrital aggregates were the main vehicles for the settling transport during the sampled time period. Phytodetrital aggregates rebound relatively easily: for rebound to occur, typically, current speeds at ~1 mab are thought to have to be at least ~7 cm s^{-1} (Lampitt, 1985; Beaulieu, 2002). Such current speeds are not unusual in the study area (Figs. 2 and 8). If it is assumed that, on the time scale of the arriving bloom (several weeks), all settling particulate mat-

ter that enters the BML rebounds and is evenly distributed and recirculated within the BML without any net degradation and other changes, the particulate matter would simply accumulate within the BML, leading to a gradual increase of the trap fluxes at 2 mab and 40 mab.

Such cumulative fluxes (F_C) within BML-affected waters were calculated for the trap time series and compared with the actually measured fluxes (F_M) within BML-affected waters. F_C was calculated by cumulatively adding the primary fluxes that were determined at 569 mab. For each trap-sampling time window, F_M was calculated as the average of the fluxes measured at 2 mab and 40 mab. However, the comparison of F_M and F_C requires consideration of the time it takes settling particles to sink from 569 mab into the bottommost 10s of meters of the water column. One approach would be to simply compare a given flux signal in the BML with the flux signal at 569 mab that was observed one week (the trap-collection interval) before the given signal at 2 or 40 mab (rather than with the 569 mab signal that was observed during the same time interval as the given flux signal at 2 or 40 mab). A settling time of 7 d over a vertical distance of 569 m would equate to a settling velocity of 81.3 m d^{-1} or 0.94 mm s^{-1}. However, at typical settling velocities of phytodetrital particles in the study region of ~100–150 m d^{-1} (Lampitt et al., 1985), the flux signal that was observed at 569 mab would only take ~ 4–6 d to reach the trap at 2 mab. Therefore, to assess a wider range of settling velocities and settling times, two other temporal offset scenarios were used to test the sensitivity of the calculations: one used the approximate minimum settling velocity of 0.50 mm s^{-1} of biogenic particulate matter with particle or aggregates sizes of a few 100s up to a few 1000s of μm (Maggi, 2013) which would relate to a time of 13.2 d it would take primary-flux particulate matter to settle from 569 mab to the seafloor; the other used an average settling velocity of 1.45 mm s^{-1} (125 m d^{-1}) which is viewed as typical for settling particulate matter in the deep ocean of the study region (Lampitt, 1985) and would make the settling particulate matter take 4.6 d to settle from 569 mab to the seafloor. To be able to work with the 0.50 mm s^{-1} and 1.45 mm s^{-1} scenarios, settling fluxes of LM and the other particulate-matter constituents (PMCs) at 569 mab were linearly interpolated between the mid-points of the relevant neighbouring trap collection intervals.

In the following, we now discuss F_M of a given PMC during a given sampling interval i, $(F_{M\_PMC})_{t=i}$, relative to F_C of that given PMC during sampling interval i-1, $(F_{C\_PMC})_{t=i-1}$. This comparison was carried out for the three settling-velocity scenarios that were outlined in the previous paragraph. The absolute timings of the 2 mab and 40 mab flux time series are used to align the comparative $(F_{M\_PMC})_{t=i}$ vs. $(F_{C\_PMC})_{t=i-1}$ time series with the barotropic TPXO tidal current-speed time series. For the TPM and LM fluxes as well as for the fluxes of the different measured biogeochemical constituents, $(F_{M\_PMC})_{t=i}$ was always lower than $(F_{C\_PMC})_{t=i-1}$; this was found for all three settling-velocity scenarios (not shown).

One possible explanation for the discrepancy between $(F_{M\_PMC})_{t=i}$ and $(F_{C\_PMC})_{t=i-1}$ could be that the near-seafloor traps at BML-affected heights above the seafloor of 2 mab and 40 mab had lower trapping efficiencies than the trap at 569 mab that is above the BML and BBL and should have trapping efficiencies near 100% ± 20% (Bacon, 1996). For the PAP area, Turnewitsch et al. (2008) compared a time series of sediment-derived non-steady state ^{234}Th fluxes into the surface sediments with trap-derived downward ^{234}Th fluxes *within* the bottommost ~570 m that were obtained from different years, seasons and heights above the seafloor. If the seafloor sediments are viewed as the 'perfect sediment trap' and the "circulating flux cell" is a viable concept, the above comparison reveals information on the trapping efficiency of the sediment traps that were deployed in very close proximity to the seafloor. On one occasion, a trap-derived downward flux at 2 mab could be directly compared with a sediment-derived flux estimate and both fluxes agreed within one-standard-deviation of methodical uncertainties. The uncertainties were high though and the conclusion that the near-seafloor traps collect quantitatively must still be treated with some caution. However, given the absence of any further and better evidence on trapping efficiencies of near-seafloor sediment traps in the study area, we base the remaining discussion in this paper on the assumption that all the sediment traps of this study captured quantitatively the downward flux of settling particulate matter. For each given substance and point in time, the half-range between the fluxes at 2 mab and 40 mab was used as a ±measure of uncertainty of the trap-derived fluxes at 2 mab and 40 mab.

The alternative explanation for the discrepancies between $(F_{C\_PMC})_{t=i-1}$ and $(F_{M\_PMC})_{t=i}$ involves (1) ultimate (irreversible) net deposition at the SWI; (2) BML- and BBL-driven and/or biologically driven changes of particle-size distribution and settling velocities through conversion of settling into suspended particulate matter; and/or (3) biogeochemically driven net conversion of particulate into dissolved material (microbially controlled degradation of organic matter, leaching and/or abiotic biomineral dissolution). Process (1) leads to a net removal of matter from the near-seafloor water column whereas processes (2) and (3) lead to transfer of settling particulate matter into suspended particulate matter and dissolved matter that are not captured (not 'seen') by the traps.

As mentioned above, on the time scales of this study (days to months), LM can be safely assumed to be chemically inert. That is, the aforementioned process (3) can be neglected for LM, and discrepancies between $(F_{M\_LM})_{t=i}$ and $(F_{C\_LM})_{t=i-1}$ have to be due to processes (1) and/or (2). Then, a time series of $R_{LM\_i,i-1} = [(F_{M\_LM})_{t=i} - (F_{M\_LM})_{t=i-1}]/[(F_{C\_LM})_{t=i-1} - (F_{C\_LM})_{t=i-2}]$ contains information on changes of the combined effects of processes (1) and (2). The $R_{LM\_i,i-1}$ calculations were carried out for the three different settling-velocity scenarios outlined above. The different main cases that can lead to high or low and to positive or negative $R_{LM\_i,i-1}$ values are summarised in Table 1. There are two main groups of cases. Case group 1 (S^{0-1}_{++}, $S^{>1}_{--}$, S^{-1-0}_{-+}, $S^{<-1}_{-+}$) reflects processes that result in the measured BBL trap flux of LM to be lower than what would be expected from the cumulative LM flux into the BBL: such processes include net deposition of LM at the SWI and/or transfer of LM from settling into suspended particles. Conversely, case group 2 (S^{0-1}_{--}, $S^{>1}_{++}$, S^{-1-0}_{+-}, $S^{<-1}_{+-}$) reflects processes that result in the measured BBL trap flux of LM to be higher than what would be expected from the cumulative LM flux into the BBL: such processes include net resettling of previously resuspended LM particles and/or transfer of suspended LM into settling particles. If, as a convention, case group 1 is allocated a negative sign and case group 2 a positive sign, the time series of $R_{LM\_i,i-1}$ takes the form shown in Fig. 12. For both case groups, increasing (more positive) values indicate a strengthening of the respective net process.

Assessing uncertainties for these calculations is difficult as it requires quantification of the trapping uncertainty. In the absence of any direct information, and to provide a starting point for this kind of uncertainty analysis, we chose the following approach to assess $R_{LM\_i,i-1}$ uncertainties. First, it was assumed that the half-difference between fluxes measured by the traps at 2 mab and 40 mab can be viewed as a measure of the ±uncertainty in trap-derived fluxes of the near-seafloor traps. Second, for the trap at 569 mab, a trapping efficiency of 100% was assumed with an uncertainty of ±20% (this is a reasonably typical value for this kind of trap away from ocean boundaries: see Bacon, 1996). Third, these uncertainties for individual flux data were then propagated through the calculations for $R_{LM\_i,i-1}$ and are shown in Fig. 12.

Table 1
Summary of cases (first column) of $R_{LM\_i,i-1} = [(F_{M\_LM})_{t=i} - (F_{M\_LM})_{t=i-1}]/[(F_{C\_LM})_{t=i-1} - (F_{C\_LM})_{t=i-2}]$ for different combinations of rates and directions of temporal change of F_C and F_M for LM. The different combinations could be allocated to two main groups of cases (last column): the first group (process 1) contains net deposition and/or transfer into suspended particles; the second group (process 2) contains net resuspension and/or transfer into settling particles. Process 1 and 2 were defined by negative and positive $R_{LM\_i,i-1}$, respectively ['×(−1)' indicates where the original $R_{LM\_i,i-1}$ had to be multiplied by −1 to conform to this convention; see text for more details]. The slope lines in columns 3 and 4 indicate temporal flux changes, defined as $(F_{M\_LM})_{t=i} - (F_{M\_LM})_{t=i-1}$ and $(F_{C\_LM})_{t=i-1} - (F_{C\_LM})_{t=i-2}$, respectively, with time progressing from left to right (the higher the slope angle from the horizontal, the higher the temporal rate of change; '+' and '−' indicate temporal flux increase and decrease, respectively). A given grey shade in column 2 indicates a specific $R_{LM\_i,i-1}$ range.

case	$R_{LM\_i,i-1}$	$(F_{M\_LM})_{t=i} - (F_{M\_LM})_{t=i-1}$		$(F_{C\_LM})_{t=i-1} - (F_{C\_LM})_{t=i-2}$		process	
S_{++}^{0-1}	$0 < R_{LM\_i,i-1} < 1$	+		+		1	(×(-1))
$S_{--}^{>1}$	$R_{LM\_i,i-1} > 1$	-		-		1	(×(-1))
S_{-+}^{-1-0}	$-1 < R_{LM\_i,i-1} < 0$	-		+		1	
$S_{-+}^{<-1}$	$R_{LM\_i,i-1} < -1$	-		+		1	
S_{--}^{0-1}	$0 < R_{LM\_i,i-1} < 1$	-		-		2	
$S_{++}^{>1}$	$R_{LM\_i,i-1} > 1$	+		+		2	
S_{+-}^{-1-0}	$-1 < R_{LM\_i,i-1} < 0$	+		-		2	(×(-1))
$S_{+-}^{<-1}$	$R_{LM\_i,i-1} < -1$	+		-		2	(×(-1))

The $R_{LM\_i,i-1}$ calculations for the three different settling-velocity scenarios revealed sensitivity of the absolute $R_{LM\_i,i-1}$ values to settling velocities (Fig. 12a–c: open and closed red symbols). However, overall, there were the same trends. The least negative $R_{LM\_i,i-1}$ values (indicating intense deposition and/or transfer into suspended particles) were encountered during deceleration out of a spring tide whereas the most negative values (indicating weak deposition and/or transfer into suspended particles) or even positive values (indicating resuspension) were encountered during acceleration into a spring tide. The time window where positive values occurred was during flow acceleration from a particularly weak neap tide into a particularly strong spring tide (Fig. 12).

Corresponding $R_{PMC\_i,i-1}$ ratios have also been calculated for the biogeochemical PMCs. Again, there was sensitivity of the absolute $R_{PMC\_i,i-1}$ values to settling velocities (Fig. 12a–c): with decreasing settling velocities, $R_{PMC\_i,i-1}$ uncertainties and the spread of $R_{PMC\_i,i-1}$ values tended to increase. However, the temporal trend of all $R_{PMC\_i,i-1}$ and $R_{LM\_i,i-1}$ values taken together is broadly similar for the three settling-speed scenarios, with more negative or even positive values during transition into a spring tide and less negative values during transition into a neap tide. And, overall, in many cases, $R_{PMC\_i,i-1}$ and $R_{LM\_i,i-1}$ values differed from each other, with $R_{PMC\_i,i-1}$ values often being more negative than corresponding $R_{LM\_i,i-1}$ values (Fig. 12).

In principle, these differences between $R_{LM\_i,i-1}$ and $R_{PMC\_i,i-1}$ could be exploited to deduce information on purely biogeochemical (rather than particle-dynamic) processes, i.e., on the aforementioned process group (3). For instance, if it is assumed that LM directly 'traces' the other non-LM PMCs in terms of processes (1) and (2), the ratios $R_{PMC/LM\_i,i-1} = (\pm R_{PMC\_i,i-1})/(\pm R_{LM\_i,i-1})$ should then reveal information on process (3). For this $R_{PMC/LM\_i,i-1}$ ratio, the eight main scenarios are summarised in Table 2, with $R_{PMC/LM} = 1$ indicating the absence of biogeochemically driven *net* conversion between settling-particulate and dissolved material (i.e., in *net* terms, the biogeochemical substances behave in the same way as LM.

When the $R_{PMC/LM\_i,i-1}$ calculations were carried out, most values were found to be negative, suggesting a prevalence of biogeochemically driven conversion of PMC into dissolved material (Table 2). And, interestingly, the $R_{PMC/LM\_i,i-1}$ calculations revealed a trend towards more intense biogeochemically driven *net* conversion of settling particulate material into dissolved material during transitions from spring into neap tides as compared to transitions from neap into spring tides. However, when error propagations were carried out for $R_{PMC/LM\_i,i-1}$ they resulted in extremely high uncertainties of some $R_{PMC/LM\_i,i-1}$ results, especially during transition from spring into neap tides. The particularly high uncertainties during transition from spring into neap tides are mainly due to low (near-zero) absolute $R_{LM\_i,i-1}$ and $R_{PMC\_i,i-1}$ values. Unfortunately, these high uncertainties made comparisons of most $R_{PMC/LM\_i,i-1}$ values impossible.

Although no *direct* evidence for a biogeochemical influence of neap/spring tidal fluid dynamics could be found in the field data, this does not rule out the possible existence of such an influence: other approaches could potentially be sufficiently sensitive and accumulate sufficiently low uncertainties to *directly* address the question of a biogeochemical influence of neap/spring tidal fluid dynamics. Moreover, above it was concluded that *intensified* deposition and/or transfer of settling into suspended particulate matter are likely to have occurred during deceleration out of a spring tide whereas *weakened* deposition (or even resuspension) and/or transfer of settling into suspended particulate matter are likely to have occurred during acceleration into a spring tide. If this finding is combined with the physical-oceanographic and fluid-dynamic information of Section 3.1 and with information from previously published empirical or theoretical relations between fluid and biogeochemical dynamics at the scale of individual particle aggregates, a conceptual and semi-quantitative picture of a mechanism can be derived that explains in an *indirect* way how neap/spring tidal flow dynamics could influence biogeochemical fluxes in the BBL. This picture will be developed in the next Section 3.4.2.

3.4.2. Possible mechanisms

The aforementioned mechanisms that influence biogeochemical decomposition involve controls on the extent to which water

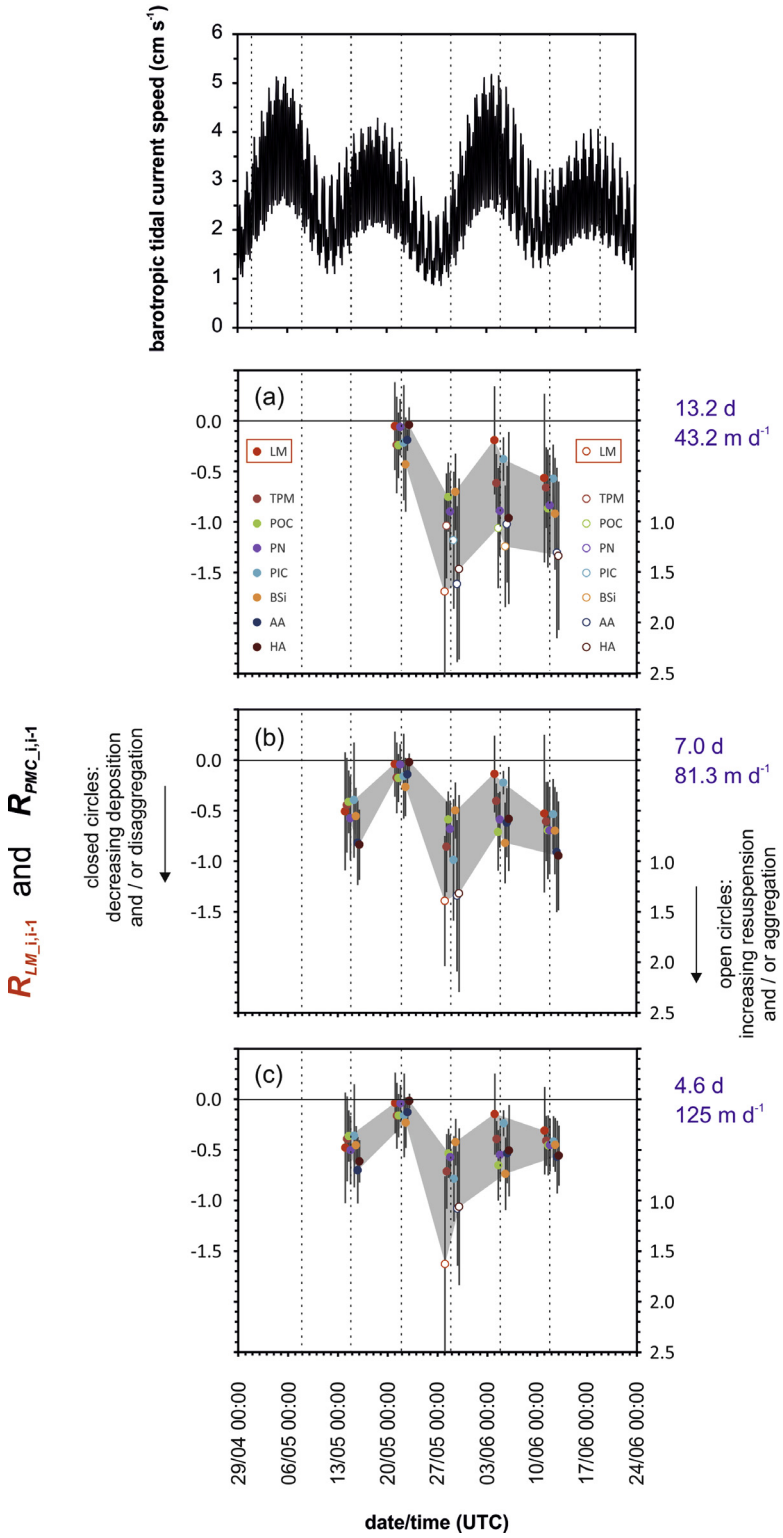

Fig. 12. Same as Fig. 9, but for the $R_{LM\_i,i-1}$ (red circles) and $R_{PMC\_i,i-1}$ ratios (all other circles). Vertical bars indicate overall uncertainties that resulted from assumed and propagated measures of the uncertainties that are associated with the measured trap-derived settling fluxes (see Section 3.4.1 for details). Left ordinates (closed circles): values <0 stand for deposition and/or disaggregation, with less negative values indicating an intensification of these processes. Right ordinates (open circles): values >0 stand for resuspension and/or aggregation, with more positive values indicating an intensification of these processes. All relevant values of $R_{LM\_i,i-1}$ and $R_{PMC\_i,i-1}$ have been adjusted by a factor of −1 if required and as explained in Table 1. Hand-drawn grey areas indicate how the ranges of average values for all $R_{LM\_i,i-1}$ and $R_{PMC\_i,i-1}$ ratios connect between successive time intervals. (a) $R_{LM\_i,i-1}$ and $R_{PMC\_i,i-1}$ calculations were carried out assuming that it took 13.2 d for the primary-flux particulate matter to settle from 569 mab to the seafloor, implying an average settling velocity of 43.2 m d^{-1} or 0.50 mm s^{-1} (the approximate minimum velocity of biogenic settling particulate matter with particle or aggregate sizes of a few 100s up to a few 1000s of µm: Maggi, 2013). Because of the comparatively long time (almost 2 trapping intervals) it takes this particulate matter to settle between 569 mab and the seafloor, no results could be calculated for 15/05/2000. (b) $R_{LM\_i,i-1}$ and $R_{PMC\_i,i-1}$ calculations were carried out assuming that it took 7.0 d (the trap collection interval) for the primary-flux particulate matter to settle from 569 mab to the seafloor, implying an average settling velocity of 81.3 m d^{-1} or 0.94 mm s^{-1}. (c) $R_{LM\_i,i-1}$ and $R_{PMC\_i,i-1}$ calculations were carried out assuming that it took 4.6 d for the primary-flux particulate matter to settle from 569 mab to the seafloor, implying an average settling velocity of 125.0 m d^{-1} or 1.45 mm s^{-1} (this velocity is viewed as typical for settling particulate matter in the deep ocean of the study region: Lampitt, 1985).

Table 2
Summary of eight possible scenarios of $R_{PMC/LM\_i,i-1} = (\pm R_{PMC\_i,i-1})/(\pm R_{LM\_i,i-1}) \neq 1$ for different combinations of 'directions' (negative or positive) of $R_{PMC\_i,i-1}$ and $R_{LM\_i,i-1}$. Deviations from $R_{PMC/LM\_i,i-1} = 1$ indicate that a given PMC behaves differently from LM. Process 1 and 2 were defined by negative and positive $R_{LM\_i,i-1}$, respectively (see Table 1). The two main types of behavioural deviations of PMC compared to the behaviour of LM are removal (R) and addition (A) of dissolved material to the settling particulate phase. By definition, negative and positive $R_{PMC/LM\_i,i-1}$ values indicate net R and net A. '×(−1)' indicates where the original $R_{PMC/LM\_i,i-1}$ had to be multiplied by −1 to conform to this convention. See text for more details.

$R_{PMC/LM\_i,i-1}$		$R_{PMC\_i,i-1}$	
		+	−
$R_{LM\_i,i-1}$	+	(1): $0 < R_{PMC/LM\_i,i-1} < 1$: **R** (×(−1))	(3): $-1 < R_{PMC/LM\_i,i-1} < 0$: **hA** (×(−1))
		(2): $R_{PMC/LM\_i,i-1} > 1$: **A**	(4): $R_{PMC/LM\_i,i-1} < -1$: **A** (×(−1))
	−	(5): $-1 < R_{PMC/LM\_i,i-1} < 0$: **R**	(7): $0 < R_{PMC/LM\_i,i-1} < 1$: **R** (×(−1))
		(6): $R_{PMC/LM\_i,i-1} < -1$: **hR**	(8): $R_{PMC/LM\_i,i-1} > 1$: **A**

(1) Net PMC resuspension and/or transfer into settling particles occur/s but are/is lower than expected from net LM resuspension and/or transfer into settling particles: this implies some form of **removal of PMC (R)** from the settling flux into the dissolved phase that does not occur for LM.
(2) Net PMC resuspension and/or transfer into settling particles occur/s and appear/s to be higher than expected from net LM resuspension and/or transfer into settling particles: this implies some form of **addition (A)** of material from the dissolved to the settling particulate phase that does not occur for LM.
(3) High net PMC deposition and/or transfer into suspended particles occurs while high net LM resuspension and/or transfer into settling particles occurs: this implies some form of **high addition (hA)** of dissolved material to the settling particulate phase that does not occur for LM.
(4) Low net PMC deposition and/or transfer into suspended particles occurs while low net LM resuspension and/or transfer into settling particles occurs: this implies some form of **addition (A)** of dissolved material to the settling particulate phase that does not occur for LM.
(5) Relatively low net PMC resuspension and/or transfer into settling particles occur/s while relatively low net LM deposition and/or transfer into suspended particles occur/s: this implies some form of **removal of PMC (R)** from the settling flux into the dissolved phase that does not occur for LM.
(6) Relatively high net PMC resuspension and/or transfer into settling particles occur/s while relatively high net LM deposition and/or transfer into suspended particles occur/s: this implies some form of **high removal of PMC (hR)** from the settling flux into the dissolved phase that does not occur for LM.
(7) Net PMC deposition and/or transfer into suspended particles occur/s but are/is higher than expected from net LM deposition and/or transfer into suspended particles: this implies some form of **removal of PMC (R)** from the settling flux into the dissolved phase that does not occur for LM.
(8) Net PMC deposition and/or transfer into suspended particles occur/s but are/is less than expected from net LM deposition and/or transfer into suspended particles: this implies some form of **addition (A)** of dissolved material to the settling particulate flux that does not occur for LM.

movements around aggregates increase the overall (diffusive + advective) transport of dissolved substances to/away from the surfaces of settling aggregates. For aerobic, microbially driven biogeochemical decomposition of organic components (here: POC, PN, AA, HA) of aggregates that move relative to the ambient water, the overall transport of dissolved oxygen to the aggregate surfaces is key: at increased speeds of the water relative to the aggregates, this overall transport should increase, leading to a reduction of diffusive-transport limitation (Kiørboe et al., 2001) and a potentially accelerated microbial biogeochemical decomposition of the organic matter. For the inorganic biogenic components (here: PIC, BSi), overall transport of the products of dissolution (here, mainly bicarbonate and silicate ions) away from the aggregate surface is key as it is a control on the extent of undersaturation right at the aggregate surface and, therefore, on the rate of dissolution. There are two main ways in which aggregates can move relative to ambient water: movements in turbulent flow and aggregate settling. In the following text and in Figs. 13–15, their relative effects will be scrutinised, followed by a discussion of the implications for BBL biogeochemistry under the influence of neap/spring oscillations.

Effects of turbulence on aggregate biogeochemistry --- For passive (neutrally buoyant, non-motile) particles in turbulent flow, Karp-Boss et al. (1996) reported relations between the dimensionless Sherwood number, *Sh*, and the dimensionless Péclet number, *Pe*. For a given substance, *Sh* is the ratio of total (diffusive + advective) mass transport to mass transport purely due to diffusion to/from a spherical body. In the turbulent context, the Péclet number,

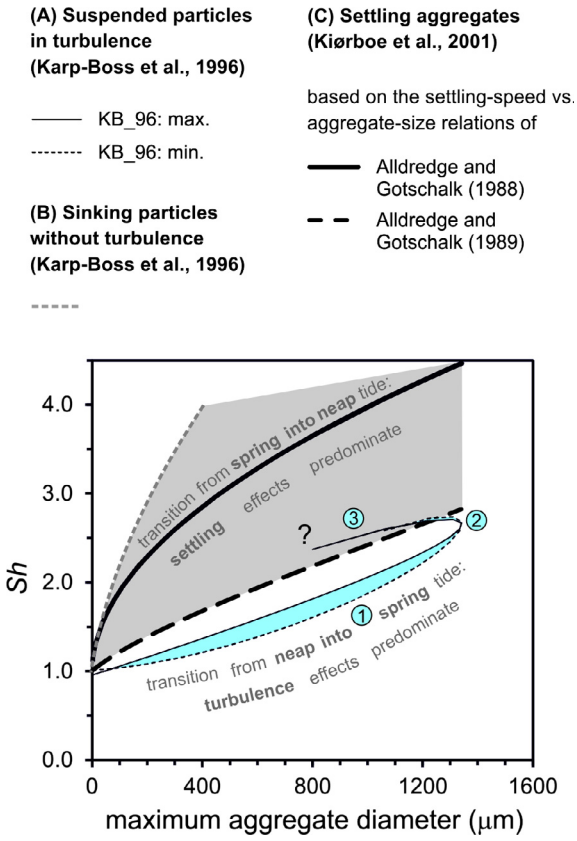

Fig. 13. Different relations between the maximum aggregate diameter ($d = 2 \times r$) and the Sherwood number, *Sh*. $Sh > 1$ indicates that a given solute is transported faster than what would be expected due to pure molecular diffusion. Two types of relations were considered to assess the effects of turbulence and particle settling on *Sh*: (A) Relations predicting *Sh* in turbulent waters for suspended (non-settling) particle aggregates (i.e., $Sh = Sh_{turb}$) (blue area); and (B, C) relations predicting *Sh* in non-turbulent waters for settling particles and aggregates (i.e., $Sh = Sh_s$) (grey area). Turbulent effects are thought to predominate during transition from neap into spring tide, whereas settling effects are thought to predominate during transition from spring into neap tide. There is evidence for a hysteresis-like behaviour of *Sh* between transitions from neap into spring tide and transitions from spring into neap tide. (A) For *particles in turbulence* (thin black lines), maximum Sh_{turb} values were estimated by $Sh_{turb} = 0.955 + 0.344\ Pe_{turb}^{1/3}$ (KB_96: max; solid thin line) and minimum values were estimated by $Sh_{turb} = 1.014 + 0.15\ Pe_{turb}^{1/2}$ (KB_96: min; dashed thin line), following Karp-Boss et al. (1996) and with turbulence-related *Pe*, Pe_{turb}, defined as $Pe_{turb} = (\varepsilon/\nu)^{1/2} r^2/D$. The graphs in this figure were calculated using a coefficient of molecular diffusion of $D = 1.8 \times 10^{-5}$ cm^2 s^{-1}, a value that is typical for dissolved oxygen in seawater. The relation between $(\varepsilon/\nu)^{1/2}$ and $r = d/2$ was approximated from Berhane et al. (1997) as $r = (-5855.3 \times (\varepsilon/\nu) + 5605.1 \times (\varepsilon/\nu)^{1/2} + 2)/2$, with r measured in μm and $(\varepsilon/\nu)^{1/2}$ in s^{-1} and with the relation being valid up to $\varepsilon \approx 10^6$ μm^2 s^{-3} (10^{-6} W kg^{-1}). ①: $\varepsilon < 10^{-7}$ W kg^{-1}; ②: $\varepsilon \approx 10^{-7}$ W kg^{-1}; ③: $\varepsilon > 10^{-7}$ W kg^{-1}. The robustness of the relationship is particularly uncertain for $\varepsilon > 10^{-7}$ W kg^{-1} ('?'). See main text for more details. (B) For *settling particles without turbulence* (grey dashed line): relationship according to Karp-Boss et al. (1996), with particles settling according to Stokes' law, with an excess mass density of the particles relative to water of 0.01 g cm^{-3}, and with a molecular diffusion coefficient of 10^{-5} cm^2 s^{-1}. (C) For *settling aggregates* (bold black lines), two ε vs. Sh_s relationships are plotted that are defined by two different relations between aggregate diameter, d (cm), and settling speeds, U_s (cm s^{-1}): $U_s = 0.065 d^{0.26}$ according to Alldredge and Gotschalk (1988) and $U_s = 0.1d$ according to Alldredge and Gotschalk (1989). Here, Sh_s is calculated according to $Sh_s = 1 + 0.619\ Re^{0.412}\ Sc^{1/3}$, where $Re = (d/2)\ U_s/\nu$, $Sc = Pe/Re = \nu/D$ and $Pe = U_s\ d/2/D$ (Kiørboe et al., 2001).

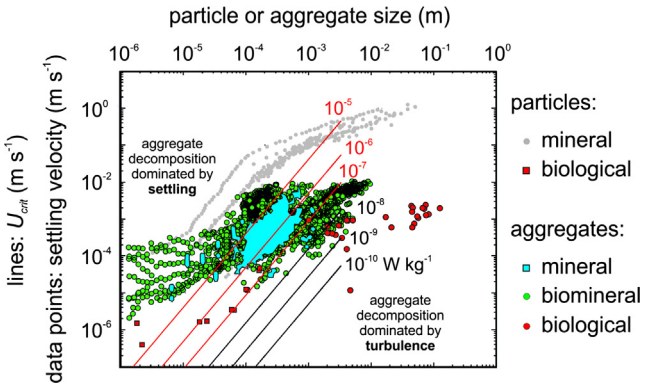

Fig. 14. Relationships between particle or aggregate sizes and settling velocities (redrawn and adapted from Maggi (2013)). Data for three main groups of particles and aggregates are shown: 'mineral' (no or only traces of organic matter (OM)), 'biomineral' (≥20% of dry mass is OM), 'biological' (≥60% of dry mass is OM; or cells only). The red and black solid lines indicate relationships between particle or aggregate size (nominal diameter, d_n) and the critical settling velocity (U_{crit}) that separates a setting in which biogeochemical decomposition is predominantly controlled by settling (upper left area of the diagram) from a setting in which biogeochemical decomposition is predominantly controlled by turbulence (lower right area of the diagram). The relationship between U_{crit} and d_n was given by Karp-Boss et al. (1996), based on Batchelor (1980): $U_{crit} = ((d_n/2)^2/D^{0.5})(\varepsilon/\nu)^{3/4}$, where D is a representative diffusion coefficient; here: 10^{-5} cm^2 s^{-1}), ε is the rate of energy dissipation, and ν is kinematic viscosity of the seawater (here assumed to be 0.0169 cm^2 s^{-1}). The relationship was calculated for six values of ε: 10^{-10}, 10^{-9}, 10^{-8}, 10^{-7}, 10^{-6}, 10^{-5} W kg^{-1}. Black lines indicate ε scenarios ($\varepsilon = 10^{-10}$, 10^{-9}, 10^{-8} W kg^{-1}) that are more likely to occur during neap tides and, in particular, in the interior ocean above the boundary layer; red lines indicate ε scenarios ($\varepsilon = 10^{-7}$, 10^{-6}, 10^{-5} W kg^{-1}) that are more likely to occur in the boundary layer and, in particular, during spring tides. (For interpretation of the references to colour in this figure legend, the reader is referred to the web version of this article.)

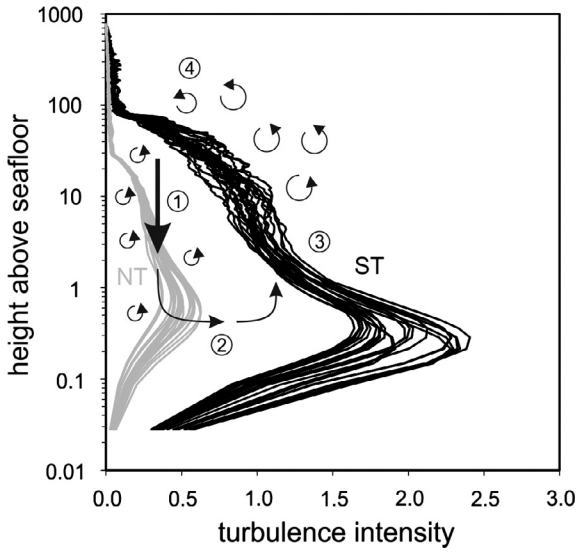

Fig. 15. Conceptual sketch of the proposed effect of neap/spring variations of turbulence intensities on particulate-matter recirculation in a deep-sea BBL. NT (grey): 26 temporally equidistant profiles of turbulence intensity for one semidiurnal cycle during neap tide; ST (black): same for spring tide. ①: During neap tide, reduced turbulence intensities foster enhanced settling of particle aggregates (in the PAP study area, reduced turbulence intensities are thought to result from intensified counter-rotation of tidal flow components and from the now *relatively* strong near-inertial clockwise flow component). ②: Settling aggregates break up in the highly turbulent waters just above the seafloor (especially in the buffer layer). ③: During transition from neap into spring tide, disaggregated material is partly injected back up into near-seafloor waters above the buffer layer (as evidenced in Fig. 8), and increasing turbulence intensities suppress settling of particulate matter and foster shear-driven re-aggregation and upward turbulent-diffusive transport of the aggregates (in the PAP study area, increased turbulence intensities are thought to result from intensified co-rotation of tidal flow components and from the now *relatively* weak near-inertial clockwise flow component); during this time interval, turbulence effects on biogeochemical aggregate decomposition and dissolution are proposed to predominate over settling effects, leading to reduced biogeochemical decomposition and dissolution. ④: During transition from spring into neap tide, turbulence intensities decrease and settling effects on biogeochemical aggregate decomposition and dissolution are proposed to predominate over turbulence effects, leading to enhanced biogeochemical decomposition (①).

Pe_{turb}, is the ratio of the rate of advection of a physical quantity by the flow to the rate of diffusion of the same quantity driven by a concentration gradient. Pe_{turb} can be defined as $Pe_{turb} = Ur/D = (\varepsilon/\nu)^{1/2}r^2/D$, where U is a characteristic free-flow velocity of the turbulent ambient waters, r is the particle radius, D is the diffusion coefficient for the dissolved substance of interest, ε is the rate of dissipation of turbulent kinetic energy, and ν is the kinematic viscosity of the ambient water. Karp-Boss et al. (1996) propose that in systems dominated by turbulence Sh would lie between minimum values defined by $Sh_{turb} = 1.014 + 0.15\ Pe_{turb}^{1/2}$ and maximum values defined by $Sh_{turb} = 0.955 + 0.344\ Pe_{turb}^{1/3}$.

It is important to note that r is not independent of ε. ε tends to increase with turbulence intensity (indirectly expressed by U) and with the rate of production of turbulent kinetic energy (e.g., Gayen and Sarkar, 2010). In much of the interior ocean, ε values range from as low as 10^{-11} W kg^{-1} up to 10^{-8} W kg^{-1}, with the majority of values lying in the range of $10^{-10} - 10^{-9}$ W kg^{-1} (Waterhouse et al., 2014). In BBLs, however, ε is thought to have the potential to reach higher. Credible information on ε very close to the seafloor (in the buffer and log layer) in the deep sea is extremely sparse but suggests ε can reach up to several 10^{-4} W kg^{-1} and possibly even up to ~10^{-3} W kg^{-1} (Gust and Weatherly, 1985). Oscillating and/or sloping boundary layers in mass-density-stratified waters appear to have a particularly high likelihood of being associated with such high ε values, at least transiently (e.g., Gayen and Sarkar, 2011).

The relation between ε and r is poorly constrained, especially when it comes to aggregates in waters of the deep open oceans (it appears to be somewhat better constrained for shelf, coastal and estuarine settings: e.g., Dyer, 1989; Berhane et al., 1997; Manning and Dyer, 1999; Burd and Jackson, 2009; Braithwaite et al., 2012). Given the lab results of Alldredge et al. (1990) and the field data of Berhane et al. (1997), it looks possible that, up to $\varepsilon \approx 10^{-7}$ W kg^{-1}, increasing ε fosters the growth of aggregates through shear-controlled aggregation and that only at ε values >10^{-7} W kg^{-1} increasing ε leads to noteworthy disaggregation. Using an approximation of the field-derived empirical relation between maximum aggregate diameter and $(\varepsilon/\nu)^{1/2}$, as shown by Berhane et al. (1997), one can relate r to $(\varepsilon/\nu)^{1/2}$ through $r = (-5855.3 \times (\varepsilon/\nu) + 5605.1 \times (\varepsilon/\nu)^{1/2} + 2)/2$, with r measured in μm and $(\varepsilon/\nu)^{1/2}$ in s^{-1}, and with the relation being valid up to $\varepsilon \approx 10^6$ μm^{2}s^{-3} (10^{-6} Wkg^{-1}).

This relation suggests that r drops quickly at >10^{-7} W kg^{-1} with increasing ε (see ② in Fig. 13), also resulting in a gradual decrease in Sh (see ③ in Fig. 13). By contrast, the study of Alldredge et al. (1990) suggests that r only drops very gradually over several orders of magnitude of increase of ε (up to ~10^{-4} W kg^{-1} were investigated). It also indicates that Sh_{turb} should continue to increase with rising ε at >10^{-7} W kg^{-1}, with r decreasing at the same time. The bottom line is that, for <10^{-7} W kg^{-1}, Sh_{turb} should always increase with increasing ε as ε and r are positively related for this range of ε (Fig. 13: ①). At >10^{-7} W kg^{-1}, the effect of increasing ε on Sh_{turb} is not well constrained and could be an increase or drop of Sh with increasing ε (hence the '?' in Fig. 13).

In summary, $Pe_{turb} = (\varepsilon/\nu)^{1/2}r^2/D$ increases with U, r and ε. And as Pe_{turb} increases, Sh_{turb} is also expected to increase, indicating enhancement of total transport to or away from an aggregate surface over transport that is purely due to molecular diffusion. Representative versions of the minimum and maximum relationships

between *Sh* and *r* are shown in Fig. 13, delimiting the blue area in the lower part of the diagram. The turbulence-controlled *Sh* vs. *r* relations (blue area in Fig. 13) suggest that in the upper BBL above the log layer (i.e., in the upper >90% of the BBL), aggregation is likely to prevail over disaggregation and *Sh* should increase with increasing ε (turbulence intensity). However, particle aggregates that enter the sublayers near the seafloor from above may partly disaggregate before either depositing at the SWI or being rebounded back into the upper BBL.

Effects of settling on aggregate biogeochemistry --- If turbulence intensities and ε are sufficiently low, particle aggregates experience increased relative advective flow due to their settling in the ambient waters (Karp-Boss et al., 1996). Based on numerical modelling, Kiørboe et al. (2001) arrive at the following expression of *Sh* for settling aggregates in water with negligible turbulence: $Sh_s = 1 + 0.619Re^{0.412}Sc^{1/3}$, where $Re = rU_s/\nu$, U_s is the settling speed (or speed of the water relative to the aggregate), and $Sc = Pe/Re = \nu/D$. This description of Sh_s is thought to be applicable to $0.1 < Re < 20$ and $30 < Pe < 50000$, i.e., it is applicable within *and* beyond the *Re* range in which Stokes' flow occurs. Two representative versions of the settling-controlled *Sh* vs. *r* relationship are shown in Fig. 13: one based on the U_s vs. *r* relationship of Alldredge and Gotschalk (1988: bold black solid line) and the other based on the U_s vs. *r* relationship of Alldredge and Gotschalk (1989: bold black dashed line). An earlier version of the settling-controlled relation between *Sh* and *Pe* (and, hence, *r*) was given by Karp-Boss et al. (1996) and has been applied here using the same range of *r* as for the relation of Kiørboe et al. (2001) (bold grey dashed line in Fig. 13). For a given *D*, all three versions of the settling-controlled *Sh* vs. *r* relationship show that Sh_s increases with increasing aggregate size (Fig. 13: the grey area indicates the *Sh* range predicted by the three versions of the settling-controlled *Sh* vs. *r* relationship).

Relative importance of turbulence and settling --- Particle aggregates in deep-sea BBLs are very likely to be experiencing both turbulence and settling most of the time in most locations. But the *relative* importance of turbulence and settling for *Sh* may vary. Based on Batchelor (1980), Karp-Boss et al. (1996) propose the following relationship as a measure to distinguish settings in which settling or turbulence predominate: $U_{crit} = (r^2/D^{0.5})(\varepsilon/\nu)^{3/4}$, where U_{crit} is a critical velocity with which the ambient waters pass a particle or aggregate and where $U > U_{crit}$ indicates predominant effects of settling on *Sh* whereas $U < U_{crit}$ indicates predominant effects of turbulence on *Sh*.

In Fig. 14, U_{crit}-vs.-*r* relationships for six different values of ε are compared with the compilation of measured particle or aggregate diameters and measured settling velocities that was published by Maggi (2013). For ε values that are typical for the interior ocean (10^{-10} – 10^{-8} W kg^{-1}), biogeochemical decomposition of large 'biological' aggregates >1000 μm is predominantly influenced by the weak turbulence and low energy dissipation; however, biogeochemical decomposition of smaller particles and aggregates is largely controlled by slow settling. Interestingly, the relative importance of settling and turbulence is particularly sensitive near $\sim10^{-7}$ W kg^{-1}: a relatively small upward shift in ε of one order of magnitude implies that biogeochemical decomposition of 'biological' particles and aggregates in the large size range of ~10–1000 μm and of an increasing fraction of 'mineral' aggregates (that are characteristic of the bulk material that was collected by this study's sediment traps) in the size range ~100–1000 μm becomes more likely to also be dominated by turbulence rather than settling. At $\varepsilon > 10^{-5}$ W kg^{-1}, biogeochemical decomposition of the whole size spectrum of 'biological' particles and aggregates of 'mineral' aggregates in the size range >10 μm is predominantly controlled by turbulence.

It, therefore, seems that the ε region around $\sim10^{-7}$ W kg^{-1} is of relevance for two key reasons: (1) above approximately 10^{-7} W kg^{-1}, phytodetrital aggregates tend to disaggregate (rather than grow) with increasing ε; and (2) when ε increases from $<10^{-7}$ W kg^{-1} to $>10^{-7}$ W kg^{-1}, predominance of turbulence over settling as a control on biogeochemical decomposition shifts from particles and aggregates in the size range >1000 μm to include the much larger size range of approximately >10 μm.

Implications for the PAP study: transition from neap into spring tide --- In the PAP study area, transition from a neap tide (here, with intensified turbulence-reducing counter-rotation of flow components) into a spring tide (here, with turbulence-enhancing co-rotation of flow components) should be associated with increasing ε. Given the only moderately high rotating and oscillating flow components and the fact that the seafloor is not sloping, it seems unlikely for the *upper* BBL and BML in this study area to reach $\varepsilon \gg 10^{-6}$ W kg^{-1}. Consequently, transition from a neap into a spring tide should lead to net aggregation and aggregate growth in the upper BBL and BML (above the log layer, if present).

Larger aggregates in non-turbulent waters tend to settle at higher speeds (Maggi, 2013; Fig. 14). But increasing turbulence intensities and ε during transition from a neap tide into a spring tide could counteract or potentially even exceed this effect on settling speed, leading to a mixing-related reduced downward flux or even a net upward transport of aggregates. The finding that there are reduced depositional fluxes as the PAP boundary-layer system moves from a neap into a spring tide (as revealed by the $R_{LM\_i,i-1}$ data; Fig. 12) indicates that the turbulence-related 'suspension' effect may indeed overwhelm any flux effect due to increased settling speeds. This, in turn, would mean that, during transition from neap into spring tides, turbulent motions would be more important for aggregate biogeochemistry than the relative advective motion of water past a settling aggregate. In other words, the aforementioned relationships that describe Sh_{turb} (blue area in Fig. 13) are likely to be more adequate for describing overall *Sh* during transitions from neap into spring tides than the relationships that describe Sh_s (grey area in Fig. 13). Moreover, the trends described in Fig. 14 also show that transition from neap into spring tides should be associated with a shift of the relevant ε isopleth towards higher values (to the upper left), leading to a *wider range* of 'biological' particle/aggregate sizes and, to a lesser extent, 'mineral' aggregate sizes (all particle/aggregate sizes to the right of the isopleth) to be predominantly affected by turbulence rather than settling.

Implications for the PAP study: transition from spring into neap tide --- By contrast, during transitions from spring into neap tide, turbulence intensities and ε are expected to decrease because of increasingly important counter-rotation of flow components. The declining turbulent motions should foster re-settling of the aggregates and net sinking speeds should increase. This means the importance of advective flow of water past settling aggregates increases whereas the importance of turbulent motions in the ambient waters decreases. In other words, the relationships that describe Sh_s (grey area in Fig. 13) are now likely to become more adequate for describing overall *Sh* than the relationships that describe Sh_{turb} (blue area in Fig. 13). This is probably particularly true because of the higher settling speeds of the larger aggregates that were 'grown' during the preceding transition from neap into spring tide.

Implications for the PAP study: comparison of the two transitions --- The final and very important factor for the proposed neap/spring mechanism that controls the biogeochemical fluxes in the near-seafloor water column now is that, for a given range of *r* (and $\varepsilon < 10^{-7}$ W kg^{-1}), Sh_s (grey area in Fig. 13) turns out to be almost always higher than Sh_{turb} (blue area in Fig. 13). Consequently, biogeochemical aggregate decomposition should tend to be higher during transitions from spring into neap tides (when settling effects are thought to be more important) than during transi-

tions from neap into spring tides (when turbulence effects are thought to be more important), leading to biogeochemical particulate-matter decomposition in near-seafloor waters whose intensity pulsates with a neap/spring frequency. It is encouraging that this notion turns out to be consistent with the aforementioned average $R_{PMC/LM\_i,i-1}$ results. However, because of the very high uncertainties of the $R_{PMC/LM\_i,i-1}$ results, this field-derived evidence is only tentative and further studies and different approaches are required to move beyond the predictive nature of this discussion.

Implications for the PAP study: closing the recirculation cell --- Finally, as mentioned above, aggregates that settle into the BL (see ① in Fig. 15) where maximum turbulent intensities occur (Fig. 5b) might partly disaggregate (see ② in Fig. 15) before depositing or rebounding back into the near-seafloor waters where they can enter further tidal cycles (see ③ in Fig. 15). Because of increased (re-)settling fluxes during transition from spring into neap tide (see ① in Fig. 15) it can be expected that more aggregates are entering the BL and disaggregate, leading to an increase into neap tides of the amount of particulate material of smaller grain sizes close to the seafloor (see ② and ③ in Fig. 15). This notion is consistent with the observed neap/spring pattern of turbidity at 1 mab (Fig. 8). This process closes the tidally driven recirculation of particulate matter in the near-seafloor waters (see ④ in Fig. 15).

4. Summary and conclusions

The main result of this study is evidence for an effect of neap/spring tidal boundary-layer fluid dynamics on particulate-matter dynamics in waters just above the abyssal seafloor. We then derived and proposed the conceptual and semi-quantitative picture of a mechanism that explains the translation of these particulate-matter dynamics into neap/spring-driven biogeochemical dynamics. At the centre of this picture is the notion that temporally varying rotational behaviour of different flow components (residual, tidal, near-inertial) translates into temporally and vertically varying turbulence intensities that then play a role in controlling particle aggregation and settling in near-seafloor waters, with implications for biogeochemical aggregate decomposition (microbially driven organic-matter breakdown, leaching and biomineral dissolution). The limited evidence so far suggests that the rotational behaviour of the different flow components may lead to oscillations in particle and biogeochemical dynamics even if total free-stream current speeds are low (<10 cm s^{-1}) and maximum speeds do not change. The main steps that led to this mechanistic picture are as follows.

(1) *Fluid-dynamic neap/spring tide differences* --- In the case of the PAP site, increasing turbulence intensity during transition from neap into spring tides is thought to result from enhanced co-rotation of flow components (rather than increasing total current speeds). And decreasing turbulence intensity during transition from spring into neap tide is thought to result from enhanced counter-rotation of flow components (rather than decreasing total current speeds). As rotational and oscillatory properties of different flow components and their temporal and vertical behaviour throughout the BBL can be subtle but crucial drivers of turbulence properties, there may be important fluid-dynamical BBL aspects *in addition to* total current speed that control particle and biogeochemical dynamics near the abyssal seafloor.

(2) *Particle dynamics: transition from neap into spring tide* --- LM data indicate that, during transition from a neap into a spring tide, deposition at the seafloor and/or disaggregation into suspended material decrease, and that during transition from a particularly weak neap tide into a strong spring tide, this trend can even lead to resuspension and/or net aggregation. Reduced deposition would result from a reduction of net settling speeds of particulate matter due to the 'suspending' effect of increasing turbulence intensity in the ambient waters, with the increase of turbulence intensity driven by intensified co-rotation of flow components. At the comparatively low expected ε values in the upper parts of an abyssal BBL (above the log layer, if present) above a flat seafloor, increased turbulence intensity would also be expected to foster aggregation, making net disaggregation an unlikely process. However, the data of this study do not allow us to infer the *relative* importance of decreasing deposition (increasing resuspension) vs. decreasing disaggregation (increasing aggregation).

(3) *Particle dynamics: transition from spring into neap tide* --- Conversely, LM data indicate that, during transition from a spring into a neap tide, deposition and/or disaggregation into suspended material increase. This trend coincided with a predicted decrease of turbulence intensity driven by intensified counter-rotation of flow components. Here, it can be concluded that, of the two loss options for settling particulate matter (deposition, disaggregation), net deposition is the more likely one: (a) given that decreasing turbulence intensities can be expected to be associated with decreasing ε, and given the likely positive relation between ε and aggregate sizes in the upper parts of an abyssal BBL (above the log layer, if present) above a flat seafloor, increased disaggregation in the upper BBL during transition from a spring into a neap tide looks much less likely to play a role than net deposition; (b) moreover, the dropping turbulence intensities would also have a decreasing 'suspending effect' on aggregates, resulting in higher net settling speeds and contributing to higher deposition. Here, an added positive effect on deposition could have resulted from increased settling speeds that are driven by a higher occurrence of aggregation due to differential settling of particles and aggregates (Burd and Jackson, 2009).

(4) *Particle dynamics: closing the recirculation cell* --- The above considerations lead to the conclusion that disaggregation is unlikely to have played an important role in the upper BBL (above the log layer, if present). However, *very close to the seafloor* (in the log layer and especially the buffer layer), ε might still reach values high enough to result in partial disaggregation and recirculation of some of the particulate material into the upper BBL, allowing for another neap/spring cycle in aggregate dynamics to commence. The turbidity time series of this study supports this notion.

(5) *Proposed mechanism for biogeochemical neap/spring-tide differences* --- The results from points (1)–(4) above were combined with information from previously published empirical and theoretical relations between fluid and biogeochemical dynamics at the scale of individual particle aggregates. This combination led to a conceptual and semi-quantitative picture of a mechanism that explains the translation of the above particulate-matter dynamics into neap/spring-driven biogeochemical dynamics. There are two main ways in which aggregates can move relative to ambient water: movements in turbulent flow and aggregate settling. The derived mechanism suggests that, for a given aggregate size, increasing turbulence at intensities that are thought to be typical for abyssal near-seafloor waters above the log layer is generally less effective in increasing biogeochemical aggregate decomposition than increasing advective flow past settling aggregates. This has the following two implications. (a) During transition from spring into neap tides, turbulence intensities are thought to decrease (point (1) above) and settling speeds are expected to increase: hence, due to the higher *relative* importance of

advective compared to turbulent flow around aggregates, an *increase* in microbially driven organic-matter breakdown and biomineral dissolution in BBL aggregates is predicted. (b) By contrast, during transition from neap into spring tides, turbulence intensities are thought to increase (point (1) above) and settling speeds are expected to decrease: therefore, due to the lower *relative* importance of turbulent compared to advective flow around aggregates, a *decrease* in microbially driven organic-matter breakdown and biomineral dissolution in BBL aggregates is predicted.

Overall, the above lines of reasoning suggest that enhanced transfer of both organic and inorganic biogenic material from settling aggregates into the dissolved phase coincided with increased deposition of aggregates at the seafloor, both occurring during transitions from spring into neap tides. That is, the intensity of biogeochemical particulate-matter decomposition in near-seafloor waters is predicted to pulsate with a neap/spring frequency. If it should turn out that different particulate-matter components have different sensitivities to the neap/spring tidal oscillations, the integrative effects of the BBL traverse of particulate matter might lead not only to quantitative but also compositional changes between primary and depositional fluxes.

Because of the very limited amount of information that is available on BBL fluid and biogeochemical dynamics in the deep sea, the development of the conceptual and semi-quantitative mechanisms that link aspects of BBL fluid and biogeochemical dynamics can only be viewed as a proposal to the reader and as a starting point for future studies. When more field-derived evidence on deep-sea BBLs becomes available it will also be possible to carry out more sophisticated uncertainty analyses that take into account aspects such as the composition of different particle size classes with differential sinking speeds, i.e., uncertainty analyses of a quality similar to the one for studies of particle and biogeochemical dynamics in the surface ocean (e.g., Burd et al., 2007,2010).

(6) *Concluding remarks* --- The results of this study support Rutgers van der Loeff and Boudreau (1997) in their conclusion that there is "no a priori reason why [near-seafloor waters] might not be a region of high biogeochemical activity". The results also add to the growing body of evidence suggesting that higher-frequency (tidal, near-inertial) fluid dynamics may be of more importance for marine particle dynamics and marine biogeochemistry than previously thought (e.g., Turnewitsch and Graf, 2003; Peine et al., 2009; Turnewitsch et al., 2008, 2013, 2014, 2016).

There is evidence for the neap/spring tidal oscillations to play a role already at relatively low total free-stream current speeds (<10 cm s^{-1}) and not only at very high primary fluxes of settling particulate matter (100s of mg $m^{-2}d^{-1}$) but already at low to moderately high primary fluxes (10s of mg $m^{-2}d^{-1}$). This, and the fact that higher-frequency (tidal, near-inertial) oscillations occur in almost all parts of the deep sea, suggest that the neap/spring tidal effects on BBL particle dynamics and potentially biogeochemical dynamics may be a spatiotemporally widespread phenomenon.

In addition to the simple factor of current speed, the specifics and subtleties of the temporal and vertical variability of the interplay of different rotational flow components in the BBL are likely to play an important role in how the primary flux from the interior ocean is translated into the depositional flux, with potential implications in the deep seas for sedimentary carbon deposition, benthic food supply and possibly even the sedimentary records of environmental change.

Acknowledgements

Funding: This work was supported by the Bundesministerium für Bildung, Wissenschaft, Forschung und Technologie (BMBF), Germany [grant number 03F0177A]; the Natural Environment Research Council (NERC), United Kingdom [grant number NE/G006415/1]; and the European Research Council (ERC), Belgium [grant number 669947]. We are grateful to Dr. Annick Vangriesheim for making available the original data of the study published by Vangriesheim et al. (2001). Michiel Rutgers van der Loeff and an anonymous reviewer provided very constructive and insightful comments that improved this paper.

References

Alldredge, A.L., Gotschalk, C., 1988. In situ settling behavior of marine snow. Limnol. Oceanogr. 33 (3), 339–351.
Alldredge, A.L., Gotschalk, C.C., 1989. Direct observations of the mass flocculation of diatom blooms: characteristics, settling velocities and formation of diatom aggregates. Deep Sea Res. 36 (2), 159–171.
Alldredge, A.L., Granata, T.C., Gotschalk, C.C., Dickey, T.D., 1990. The physical strength of marine snow and its implications for particle disaggregation in the ocean. Limnol. Oceanogr. 35 (7), 1415–1428.
Auffret, G., Khripounoff, A., Vangriesheim, A., 1994. Rapid post-bloom resuspension in the northeastern Atlantic. Deep-Sea Res. I 41 (5/6), 925–939.
Bacon, M.P., 1996. Evaluation of sediment traps with naturally occurring radionuclides. In: Ittekkot, V., Schäfer, P., Honjo, S., Depetris, P.J. (Eds.), Particle Flux in the Ocean. SCOPE. John Wiley & Sons Ltd, New York, pp. 85–90.
Bacon, M.P., Rutgers van der Loeff, M.M., 1989. Removal of ^{234}Th by scavenging in the bottom nepheloid layer of the ocean. Earth Planet. Sci. Lett. 92, 157–164.
Batchelor, G.K., 1980. Mass transfer from small particles suspended in turbulent fluid. J. Fluid Mech. 98 (3), 609–623.
Beaulieu, S.E., 2002. Accumulation and fate of phytodetritus on the sea floor. Oceanogr. Mar. Biol. Annu. Rev. 40, 171–232.
Berhane, I., Sternberg, R.W., Kineke, C.G., Milligan, T.G., Kranck, K., 1997. The variability of suspended aggregates on the Amazon Continental Shelf. Cont. Shelf Res. 17 (3), 267–285.
Berner, R.A., 2004. The Phanerozoic Carbon Cycle: CO_2 and O_2. Oxford University Press, Oxford.
Boetius, A., Springer, B., Petry, C., 2000. Microbial activity and particulate matter in the benthic nepheloid layer (BNL) of the deep Arabian Sea. Deep-Sea Res. II 47, 2687–2706.
Boudreau, B.P., Jørgensen, B.B., 2001. The Benthic Boundary Layer. Oxford University Press, Oxford.
Braithwaite, K.M., Bowers, D.G., Nimmo Smith, W.A.M., 2012. Controls on floc growth in an energetic tidal channel. J. Geophys. Res. 117, C02024.
Burd, A.B., Jackson, G.A., 2009. Particle aggregation. Ann. Rev. Mar. Sci. 1, 65–90. http://dx.doi.org/10.1146/annurev.marine.010908.163904.
Burd, A.B., Jackson, G.A., Moran, S.B., 2007. The role of the particle size spectrum in estimating POC fluxes from ^{234}Th/^{238}U disequilibrium. Deep-Sea Res. I 54, 897–918.
Burd, A.B., Hansell, D.A., Steinberg, D.K., Anderson, T.R., Arístegui, J., Baltar, F., Beaupré, S.R., Buesseler, K.O., DeHairs, F., Jackson, G.A., Kadko, D.C., Koppelmann, R., Lampitt, R.S., Nagata, T., Reinthaler, T., Robinson, C., Robison, B.H., Tamburini, C., Tanaka, T., 2010. Assessing the apparent imbalance between geochemical and biochemical indicators of meso- and bathypelagic biological activity: what the @$#! is wrong with present calculations of carbon budgets? Deep-Sea Res. II 57, 1557–1571.
Chapman, D.C., Haidvogel, D.B., 1992. Formation of Taylor caps over a tall isolated seamount in a stratified ocean. Geophys. Astrophys. Fluid Dyn. 64, 31–65.
Cheng, N.-S., Law, A.W.-K., 2003. Fluctuations of turbulent bed shear stress. J. Eng. Mech. 129 (1), 126–130.
DeMaster, D.J., Brewster, D.C., McKee, B.A., Nittrouer, C.A., 1991. Rates of particle scavenging, sediment reworking and longitudinal ripple formation at the HEBBLE site based on measurements of ^{234}Th and ^{210}Pb. Mar. Geol. 99, 423–444.
Dyer, K.R., 1989. Sediment processes in estuaries: future research requirements. J. Geophys. Res. 94 (C10), 14327–14339.
Egbert, G.D., Erofeeva, S., 2002. Efficient inverse modeling of barotropic ocean tides. J. Atmosph. Ocean. Technol. 19, 183–204.
Gage, J.D., Tyler, P.A., 1991. Deep-Sea Biology - A Natural History of Organisms at the Deep-Sea Floor. Cambridge University Press, Cambridge.
Gardner, W.D., Southard, J.B., Hollister, C.D., 1985. Sedimentation, resuspension and chemistry of particles in the Northwest Atlantic. Mar. Geol. 65, 199–242.
Gardner, W.D., Walsh, I.D., 1990. Distribution of macroaggregates and fine-grained particles across a continental margin and their potential role in fluxes. Deep-Sea Res. 37 (3), 401–411.
Gaye-Haake, B., Lahajnar, N., Emeis, K.-C., Unger, D., Rixen, T., Suthhof, A., Ramaswamy, V., Schulz, H., Paropkari, A.L., Guptha, M.V.S., Ittekkot, V., 2005.

Stable nitrogen isotopic ratios of sinking particles and sediments from the northern Indian Ocean. Mar. Chem. 96, 243–255.
Gayen, B., Sarkar, S., 2010. Turbulence during the generation of internal tide on a critical slope. Phys. Rev. Lett. 104 (21), 218502.
Gayen, B., Sarkar, S., 2011. Boundary mixing by density overturns in an internal tidal beam. Geophys. Res. Lett. 38, L14608. http://dx.doi.org/10.1029/2011GL048135.
Gross, T.F., Williams III, A.J., Grant, W.D., 1986. Long-term in situ calculations of kinetic energy and Reynolds stress in a deep sea boundary layer. J. Geophys. Res. 91 (C7), 8461–8469.
Gust, G., Weatherly, G.L., 1985. Velocities, turbulence, and skin friction in a deep-sea logarithmic layer. J. Geophys. Res. 90 (C3), 4779–4792.
Honjo, S., Manganini, S.J., Cole, J.J., 1982. Sedimentation of biogenic matter in the deep ocean. Deep-Sea Res. 29 (5A), 609–625.
Karp-Boss, L., Boss, E., Jumars, P.A., 1996. Nutrient fluxes to planktonic osmotrophs in the presence of fluid motion. Oceanogr. Mar. Biol. Annu. Rev. 34, 71–107.
Kiørboe, T., Ploug, H., Thygesen, U.H., 2001. Fluid motion and solute distribution around sinking aggregates. I. Small-scale fluxes and heterogeneity of nutrients in the pelagic environment. Mar. Ecol. Prog. Ser. 211, 1–13.
Kump, L.R., Kasting, J.F., Crane, R.G., 2004. The Earth System. Pearson Prentice Hall.
Lahajnar, N., Wiesner, M.G., Gaye, B., 2007. Fluxes of amino acids and hexosamines to the deep South China Sea. Deep-Sea Res. I 54, 2120–2144.
Lampitt, R.S., 1985. Evidence for the seasonal deposition of detritus to the deep-sea floor and its subsequent resuspension. Deep-Sea Res. 32 (8), 885–897.
Lampitt, R.S., Newton, P.P., Jickells, T.D., Thomson, J., King, P., 2000. Near-bottom particle flux in the abyssal northeast Atlantic. Deep-Sea Res. II 47, 2051–2071.
Lorke, A., Umlauf, L., Jonas, T., Wüest, A., 2002. Dynamics of turbulence in low-speed oscillating bottom-boundary layers of stratified basins. Environ. Fluid Mech. 2, 291–313.
Lorke, A., Müller, B., Maerki, M., Wüest, A., 2003. Breathing sediments: the control of diffusive transport across the sediment–water interface by periodic boundary-layer turbulence. Limnol. Oceanogr. 48 (6), 2077–2085.
Maggi, F., 2013. The settling velocity of mineral, biomineral, and biological particles and aggregates in water. J. Geophys. Res.: Oceans 118, 2118–2132.
Manning, A.J., Dyer, K.R., 1999. A laboratory examination of floc characteristics with regard to turbulent shearing. Mar. Geol. 160, 147–170.
McCave, I.N., 1986. Local and global aspects of the bottom nepheloid layers in the world ocean. Neth. J. Sea Res. 20 (2/3), 167–181.
Mortlock, R.A., Froelich, P.N., 1989. A simple method for the rapid determination of biogenic opal in pelagic marine sediments. Deep-Sea Res. 36 (9), 1415–1426.
Munk, W., Snodgrass, F., Wimbush, M., 1970. Tides off-shore: transition from California coastal to deep-sea waters. Geophys. Fluid Dyn. 1, 161–235.
Nieuwenhuize, J., Maas, Y.E.M., Middelburg, J.J., 1994. Rapid analysis of organic carbon and nitrogen in particulate materials. Mar. Chem. 45, 217–224.
Pak, H., 1983. Fluctuations of beam-attenuation coefficient in the lowest 2 m on the continental rise off Nova Scotia. Mar. Geol. 51 (1–2), 77–97.
Passow, U., 2002. Transparent exopolymer particles (TEP) in aquatic environments. Prog. Oceanogr. 55, 287–333.
Peine, F., Turnewitsch, R., Mohn, C., Reichelt, T., Springer, B., Kaufmann, M., 2009. The importance of tides for sediment dynamics in the deep sea – evidence from the particulate-matter tracer ^{234}Th in deep-sea environments with different tidal forcing. Deep-Sea Res. I 56, 1182–1202.
Rowe, G.T., Staresinic, N., 1979. Sources of organic matter to the deep-sea benthos. Ambio Spec. Rep. – Deep Sea: Ecol. Exploit. 6, 19–23.
Rutgers van der Loeff, M.M., Boudreau, B.P., 1997. The effect of resuspension on chemical exchanges at the sediment-water interface in the deep sea – a modelling and natural radiotracer approach. J. Mar. Syst. 11, 305–342.
Sakamoto, K., Akitomo, K., 2009. The tidally induced bottom boundary layer in the rotating frame: development of the turbulent mixed layer under stratification. J. Fluid Mech. 619, 235–259.
Smith Jr., K.L., Carlucci, A.F., Williams, P.M., Heinrichs, S.M., Baldwin, R.J., Craven, D. B., 1986. Zooplankton and bacterioplankton of an abyssal benthic boundary layer: in situ rates of metabolism. Oceanol. Acta 9 (1), 47–55.
Smith Jr., K.L., 1992. Benthic boundary layer communities and carbon cycling at abyssal depths in the central North Pacific. Limnol. Oceanogr. 37 (5), 1034–1056.
Taylor, J.R., Sarkar, S., 2007. Internal gravity waves generated by a turbulent bottom Ekman layer. J. Fluid Mech. 590, 331–354.
Turner, J.T., 2002. Zooplankton fecal pellets, marine snow and sinking phytoplankton blooms. Aquat. Microb. Ecol. 27, 57–102.
Turner, J.T., 2015. Zooplankton fecal pellets, marine snow, phytodetritus and the ocean's biological pump. Prog. Oceanogr. 130, 205–248.
Turnewitsch, R., Springer, B.M., 2001. Do bottom mixed layers influence ^{234}Th dynamics in the abyssal near-bottom water column? Deep-Sea Res. I 48, 1279–1307.
Turnewitsch, R., Graf, G., 2003. Variability of particulate seawater properties related to bottom mixed layer-associated internal waves in shallow water on a time scale of hours. Limnol. Oceanogr. 48 (3), 1254–1264.
Turnewitsch, R., Reyss, J.-L., Nycander, J., Waniek, J.J., Lampitt, R.S., 2008. Internal tides and sediment dynamics in the deep sea — evidence from radioactive ^{234}Th/^{238}U disequilibria. Deep-Sea Res. I 55, 1727–1747.
Turnewitsch, R., Falahat, S., Nycander, J., Dale, A., Scott, R.B., Furnival, D., 2013. Deep-sea fluid and sediment dynamics – influence of hill- to seamount-scale seafloor topography. Earth Sci. Rev. 127, 203–241.
Turnewitsch, R., Falahat, S., Stehlikova, J., Oguri, K., Glud, R.N., Middelboe, M., Kitazato, H., Wenzhöfer, F., Ando, K., Fujio, S., Yanagimoto, D., 2014. Recent sediment dynamics in hadal trenches: evidence for the influence of higher-frequency (tidal, near-inertial) fluid dynamics. Deep-Sea Res. I 90, 125–138.
Turnewitsch, R., Lahajnar, N., Haeckel, M., Christiansen, B., 2015. An abyssal hill fractionates organic and inorganic matter in deep-sea surface sediments. Geophys. Res. Lett. 42. http://dx.doi.org/10.1002/2015GL065658.
Turnewitsch, R., Dumont, M., Kiriakoulakis, K., Legg, S., Mohn, C., Peine, F., Wolff, G., 2016. Tidal influence on particulate organic carbon export fluxes around a tall seamount. Prog. Oceanogr. 149, 189–213.
Vangriesheim, A., Khripounoff, A., 1990. Near-bottom particle concentration and flux: temporal variations observed with sediment traps and nephelometer on the Meriadzek Terrace, Bay of Biscay. Prog. Oceanogr. 24, 103–116.
Vangriesheim, A., Springer, B., Crassous, P., 2001. Temporal variability of near-bottom particle resuspension and dynamics at the Porcupine Abyssal Plain, Northeast Atlantic. Prog. Oceanogr. 50, 123–145.
Verardo, D.J., Froelich, P.N., McIntyre, A., 1990. Determination of organic carbon and nitrogen in marine sediments using the Carlo Erba NA-1500 Analyzer. Deep-Sea Res. 37 (1), 157–165.
Walsh, I., Fisher, K., Murray, D., Dymond, J., 1988. Evidence for resuspension of rebound particles from near-bottom sediment traps. Deep-Sea Res. 35 (1), 59–70.
Walsh, I.D., 1992. Large aggregate flux and fate at the seafloor: diagensis during the rebound process. In: Rowe, G.T., Pariente, V. (Eds.), Deep-Sea Food Chains and the Global Carbon Cycle. Kluwer Academic Publishers, pp. 365–373.
Walsh, I.D., Gardner, W.D., 1992. A comparison of aggregate profiles with sediment trap fluxes. Deep-Sea Res. 39 (11/12), 1817–1834.
Waterhouse, A.F., MacKinnon, J.A., Nash, J.D., Alford, M.H., Kunze, E., Simmons, H.L., Polzin, K.L., St Laurent, L.C., Sun, O.M., Pinkel, R., Talley, L.D., Whalen, C.B., Huussen, T.N., Carter, G.S., Fer, I., Waterman, S., Naveira-Garabato, A.C., Sanford, T.B., Lee, C.M., 2014. Global patterns of diapycnal mixing from measurements of the turbulent dissipation rate. J. Phys. Oceanogr. 44, 1854–1872. http://dx.doi.org/10.1175/jpo-d-13-0104.1.
Weatherly, G.L., Blumsack, S.L., Bird, A.A., 1980. On the effect of diurnal tidal currents in determining the thickness of the turbulent Ekman bottom boundary layer. J. Phys. Oceanogr. 10, 297–300.
Wimbush, M., Munk, W., 1970. The benthic boundary layer. In: Maxwell, A.E. (Ed.), The Sea, vol. 4. Wiley-Interscience, New York, pp. 731–758.